ANNUAL REVIEWS

Annual Review of Biomedical Engineering

Current Advances in Photoactive Agents for Cancer Imaging and Therapy

Deanna Broadwater,[1] Hyllana C.D. Medeiros,[1] Richard R. Lunt,[2,3] and Sophia Y. Lunt[1,2]

[1]Department of Biochemistry and Molecular Biology, Michigan State University, East Lansing, Michigan 48824, USA

[2]Department of Chemical Engineering and Materials Science, Michigan State University, East Lansing, Michigan 48824, USA; email: sophia@msu.edu, rlunt@msu.edu

[3]Department of Physics and Astronomy, Michigan State University, East Lansing, Michigan 48824, USA

Annu. Rev. Biomed. Eng. 2021. 23:29–60

The *Annual Review of Biomedical Engineering* is online at bioeng.annualreviews.org

https://doi.org/10.1146/annurev-bioeng-122019-115833

Keywords

fluorescent, phosphorescent, luminescent dyes, photoactive agent, theranostics, image-guided surgery, photodynamic therapy, photothermal therapy, cancer therapy

Abstract

Photoactive agents are promising complements for both early diagnosis and targeted treatment of cancer. The dual combination of diagnostics and therapeutics is known as theranostics. Photoactive theranostic agents are activated by a specific wavelength of light and emit another wavelength, which can be detected for imaging tumors, used to generate reactive oxygen species for ablating tumors, or both. Photodynamic therapy (PDT) combines photosensitizer (PS) accumulation and site-directed light irradiation for simultaneous imaging diagnostics and spatially targeted therapy. Although utilized since the early 1900s, advances in the fields of cancer biology, materials science, and nanomedicine have expanded photoactive agents to modern medical treatments. In this review we summarize the origins of PDT and the subsequent generations of PSs and analyze seminal research contributions that have provided insight into rational PS design, such as photophysics, modes of cell death, tumor-targeting mechanisms, and light dosing regimens. We highlight optimizable parameters that, with further exploration, can expand clinical applications of photoactive agents to revolutionize cancer diagnostics and treatment.

Contents

1. BACKGROUND

Photoactive agents are materials that absorb light and transform this energy into heat, luminescence, or excited reactive species. Photoactive compounds can be fluorescent (e.g., cyanines), phosphorescent (e.g., porphyrins and phthalocyanines), both fluorescent and phosphorescent (rare), or neither (dark—not luminescent). A dark photoactive compound without luminescence can still generate heat and chemically reactive species. Luminescent agents are generally composed of phosphorescent or fluorescent emitters, depending on the spin states involved in the emission process; phosphors generally exhibit long-lived (microseconds to milliseconds) luminescence from excited triplet states, whereas fluorophores exhibit short-lived (picoseconds to nanoseconds) luminescence from excited singlet states. Fluorescent and phosphorescent dyes, which absorb light of a specific wavelength and emit light of a different wavelength, offer great potential as both diagnostic and therapeutic agents for cancer treatment. These dyes can be utilized as a photosensitizer (PS) for phototherapy, in which light is used to activate the PS to induce biological damage, a technique commonly known as phototherapy. In the cancer field, phototherapy is a promising minimally invasive alternative to traditional chemotherapy, radiotherapy, and surgical intervention and can be used to treat a variety of cancers (1, 2). As PSs have advanced, they can now also be employed as contrast agents for tumor imaging; this combined application of therapy and diagnostics is commonly termed theranostics (3). Luminescent theranostic agents increase the precision and effectiveness of treatment, as they can detect and treat the tumor while monitoring the pharmacokinetics and pharmacodynamics of the PS injected into the patient (4). This review focuses on the clinical use of PSs as theranostic agents in cancer therapy.

PS: photosensitizer

The first use of phototherapy was reported over 3,000 years ago, when ancient Egyptian, Indian, and Chinese civilizations applied light to treat different diseases, including psoriasis, rickets, and vitiligo. Treatments for these diseases generally consisted of ingesting plant and seed extracts

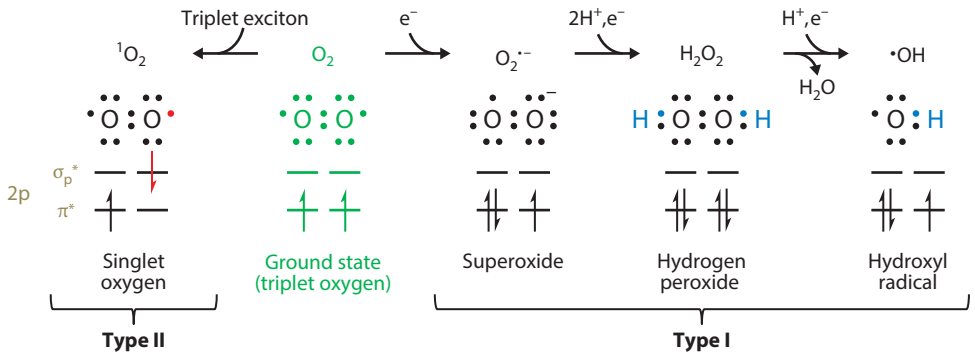

Figure 1

Common reactive oxygen species (ROS) generated during photodynamic therapy. Type I photoreactions lead to electron transfer, reacting with oxygen to generate superoxide ($O_2\cdot^-$), which can further react to generate hydrogen peroxide (H_2O_2) and hydroxyl radicals (·OH). In type II photoreactions, an excited triplet exciton is transferred to the triplet ground state oxygen, generating a highly reactive singlet state oxygen. Collectively, these ROS react with cellular components to induce damage by cleaving, oxidizing, and oxygenating biomolecules.

followed by exposure to sunlight (5, 6). Modern phototherapy began with Niels Ryberg Finsen, the father of ultraviolet therapy. In 1903, Finsen received the Nobel Prize in Physiology or Medicine for using short-wavelength light, the Finsen lamp, to treat lupus vulgaris and helped bring phototherapy to mainstream medicine. In 1907, Hermann von Tappeiner and Albert Jodlbauer introduced the term photodynamic action to describe this phenomenon (7), and photodynamic therapy (PDT) is now synonymous with phototherapy.

Agents with distinct mechanisms based on photothermal therapy (PTT) and PDT have been developed. These agents have been used against several targets including tumor tissues, bacteria, and fungi. To cause cell death, the PS generates either heat for PTT or excessive reactive oxygen species (ROS) for PDT (8). In PTT, the heat generated through the PS agent increases the temperature of the surrounding environment, ablating cells through either necrosis or apoptosis depending on the irradiation level (9). PDT requires three basic elements: a PS, light, and bioavailable oxygen in the tissue being treated. The PS absorbs a photon, transforming it from the ground singlet state to an excited singlet state, and then transfers this energy to form ROS. Often there is an intermediate step in which the excited PS first transfers the energy to a triplet state on the PS prior to transferring the energy to form a ROS. The generation of ROS is based on two different photochemical reaction processes, type I and type II PDT. Type I PDT involves an electron transfer reaction between the PS in the singlet excited state with cellular components and the triplet ground state oxygen (O_2), forming free radicals including superoxide anion ($O_2\cdot^-$), hydrogen peroxide (H_2O_2), and hydroxyl radicals (·OH) (10). In type II PDT, an excited triplet state on the PS transfers its energy directly to oxygen, converting the (O_2) triplet ground state to a reactive singlet oxygen ($^1O_2$) excited state, which can cleave many organic carbon-carbon bonds or can subsequently generate other known ROS (6, 11) (**Figure 1**). These type II photoreactions require PSs (such as phosphors) with highly efficient intersystem crossing to form triplet exciton species.

Ideal chemical properties for a theranostic PS include high extinction coefficients, chemical stability, water solubility, and long wavelengths for optimal tissue penetrance. Longer wavelengths of light are not as readily absorbed by biological endogenous fluorophores, leading to decreased light scatter and autofluorescence while improving penetrance and resolution, respectively. In biological contexts, an ideal PS should accumulate in tumor tissue while rapidly clearing from

PDT: photodynamic therapy

PTT: photothermal therapy

ROS: reactive oxygen species

the rest of the body. It should also avoid forming toxic secondary metabolites, be nonmutagenic, and display high phototoxicity (toxicity with light activation) with low cytotoxicity (toxicity in the dark) (12).

ALA: aminolevulinic acid

PDT has several clinical uses outside of cancer. The facile and immediate delivery of PS and light is ideal for the treatment of superficial dermatologic diseases. It can be used to treat various skin disorders, such as actinic keratosis, photorejuvenation, warts, and acne (13). Phototherapy is also effective for treating infectious diseases. At the beginning of the twentieth century, the first demonstration of photodynamic effect against microorganisms was described by Raab (14), when he used acridine orange and light to induce the death of a paramecium. In 1960, Macmillan and colleagues (15) showed the efficiency of toluidine blue against microorganisms such as bacteria, algae, and yeast. Since the 1990s, studies have shown the efficiency of PDT against microorganisms, and due to microbial resistance to many antibiotics/biocides, photodynamic inactivation and PDT are alternative treatments against bacteria such as *Helicobacter pylori*, *Staphylococcus aureus*, and *Escherichia coli* (16, 17). PDT can also be used to treat fungal and viral infections (18). For example, human papillomavirus infections, which cause genital warts (condyloma acuminate) and increase risk for cervical cancer, can be treated with PDT by using a porphyrin precursor, aminolevulinic acid (ALA) (19, 20).

The US Food and Drug Administration (FDA) has approved several PSs. An overview of first-, second-, and third-generation PSs is shown in **Figure 2**, and their characteristics are summarized in **Table 1**. For cancer treatment, most FDA-approved agents for PDT are based on the first-generation PS, porfimer sodium (Photofrin), a ROS-forming PS that is still in use today. PSs can induce a variety of effects, including ROS generation, ligand dissociation, toxic chemical reactions independent of oxygen, and PTT. This review focuses specifically on PSs for oxygen-dependent PDT, as they have had the most clinical success and are therefore more widely explored. Unlike PTT, which can damage adjoining tissues with high doses of laser irradiation, PDT can be repeated many times at the same site if needed. Furthermore, toxicity from oxygen-dependent PDT is the most tunable, allowing precise control of cellular toxicity to mitigate off-site tissue damage. Though important, advances made with alternative PSs are outside the scope of this review. We focus on summarizing the foundation of traditional PDT therapy and clinically approved PSs, with particular emphasis on clinical criteria such as dosage, biological indications, light delivery, and potential combinatorial therapies. By highlighting advances in the field, we aim to identify key areas where further research is necessary for the extension of photoactive theranostic agents to a wider range of cancer types in order to improve diagnostics, therapy, and overall patient outcomes.

2. CLINICAL INDICATIONS

Clinically, fluorescent agents are used for early diagnostics, as intraoperative markers in surgical resection, and for direct tumor treatment via PDT. Currently, PDT with various PSs is clinically approved for obstructive esophageal and lung cancers (worldwide), high-grade dysplasia in Barrett's esophagus (worldwide), mild to moderate actinic keratosis (worldwide), basal cell carcinoma (worldwide), advanced head and neck cancer (European Union), cutaneous T cell lymphoma (European Union), biliary tract cancer (European Union), and prostate cancer (European Union). These clinically approved PSs are summarized in **Table 2** (21, 22). Although several clinical trials have shown effective results, PDT has had a slow transition to frontline cancer treatment. PDT is currently utilized for early intervention of neoplasms or for palliative care (23). PDT is not yet appropriate for major tumor debulking due to the physical limitations of light penetrance and hypoxia common in large tumors (24). Work in the past 10 years has pushed PDT development, demonstrating its use for first-line treatment for small, centrally located tumors, inoperable or widely disseminated tumors, cancers with a high rate of recurrence, and metastasis (23, 25). PDT

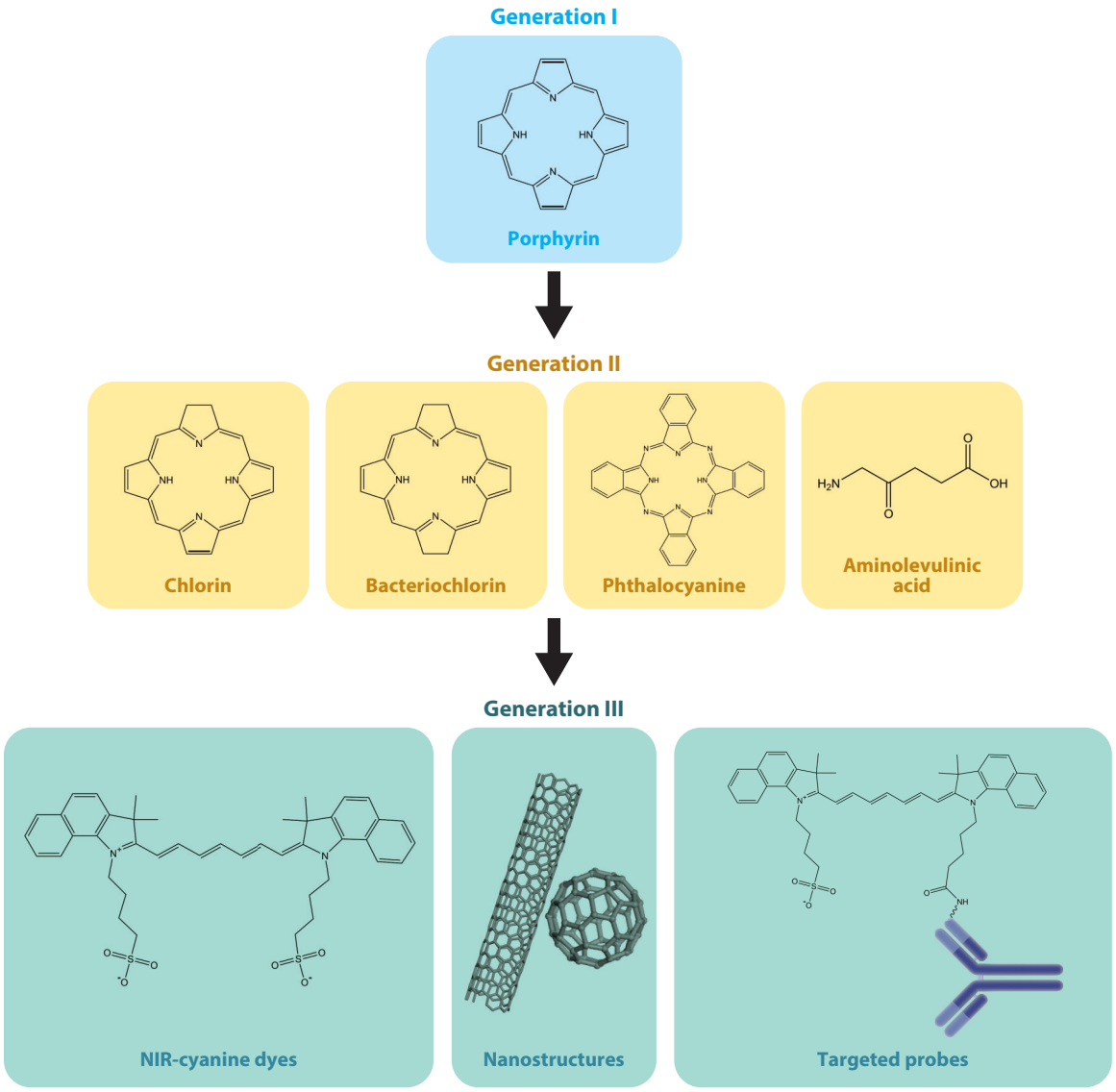

Figure 2

Overview of the three generations of photosensitizers (PSs). First-generation PSs are porphyrins, most notably Photofrin. Second-generation PSs include chlorins, bacteriochlorins, phthalocyanines, and aminolevulinic acid prodrugs. Structural differences between porphyrin, chlorin, and bacteriochlorin are highlighted with double bonds in boldface. Third-generation PSs include near-IR (NIR)-cyanine dyes, such as indocyanine green (ICG), and targeted PSs incorporated into nanostructures or bound to tumor-binding moieties, such as ICG-antibody conjugates.

has the potential to become a potent frontline cancer treatment due to its ability to increase drug delivery, induce cancer cell resensitization to traditional therapies, and trigger the body's antitumor immune response.

In addition to acting as direct antitumor agents, fluorescent molecules are used as real-time imaging probes. Many fluorescent-guided surgery (FGS) trials are utilizing PSs as real-time

Table 1 Overview of photosensitizer generations

	Advances	Absorption peak (nm)	Targeting	Mode of action	Structure	Clinical significance	Limitations
First generation	NA	630	Passive	Tumor apoptosis	Oligomeric mixture	Established PDT as a cancer therapy	Low light penetration, skin photosensitivity, poor tissue selectivity, low photostability
Second generation	Deeper wavelength absorption, increased $^1O_2$ generation	630–750	Passive	Tumor apoptosis and necrosis through vasculature destruction	Monomeric	Expanded PDT to a broader range of cancer types	Insolubility, inadequate tumor targeting, incomplete tumor regression
Third generation	Active targeting, multimodal nanodelivery platforms, advanced optical properties	>700	Active	Combinatorial therapies with PDT, PTT, and chemotherapy	Conjugated to targeting moieties and nanostructures	Aims to establish PDT as a frontline cancer therapy	Biocompatibility, aggregation-caused quenching, inadequate clinical data

Abbreviations: NA, not applicable; PDT, photodynamic therapy; PTT, photothermal therapy.

markers for tumor margins during surgery, allowing physicians to assess tumor growth, aggressiveness, and possible metastasis during tumor debulking. Biopsies can be collected from the stained tumor for fluorescent histological analysis of specific tumor markers, allowing more precise diagnoses in order to determine appropriate treatment strategies (26). Indocyanine green (ICG) is commonly used for sentinel lymph node (SLN) mapping to detect metastasis, and it is also being assessed in clinical trials for improving complete surgical resection in pancreatic, breast, liver, and brain cancers (27–30). This is termed photodynamic diagnostics and has also been applied in bladder cancer with Hexvix (an ALA analog) to identify masses that were initially missed by visual tumor identification during surgery (26). Gliolan, another ALA analog, improved complete surgical resection and progression-free survival in malignant glioma in a randomized, controlled phase III trial and is now approved in the European Union, Japan, and Australia (31, 32). FGS outcomes can also be improved when followed by intraoperative PDT. For example, in a phase II clinical trial for patients with malignant brain tumors, the debulked tumor site was irradiated with excitatory wavelengths following FGS, reducing incomplete resection by PDT-induced phototoxicity of the leading tumor edge, a site commonly missed during surgical removal of tumor tissue. This strategy reduced recurrence and had a 95.5% 12-month overall survival rate with minimal side effects. This finding shows that PDT can be used to delineate tumor margins and protect against recurrence (33, 34). Additionally, PDT has been widely studied as a neoadjuvant therapy; for example, preoperative PDT in non-small-cell lung cancer can increase the number of potential surgery candidates and improve resection completeness (35, 36).

ICG: indocyanine green

3. FIRST-GENERATION PHOTOSENSITIZERS

First-generation PSs are hematoporphyrins, a heterocyclic macrocycle composed of four interconnected pyrrole subunits derived from hemin. Purified oligomeric mixtures of hematoporphyrins

Table 2 Clinically relevant photosensitizers

Photosensitizer (brand name)	Chemical family	Localization tissue/cell	Mode of action	Absorption peak (nm)	Cancer type[a]	Year approved	Country	National Clinical Trial no.[b]	Reference(s)
Clinically approved									
Porfimer sodium (Photofrin)	Porphyrin	Tumor and vasculature/ mitochondria and lysosomes	Vasculature collapse and tumor apoptosis/ necrosis	630	**Lung**, **esophageal**, bile duct, bladder, brain, ovarian, breast, skin, pancreatic, metastatic	1993	United States, Canada, Japan, Russia, China, European Union	NCT01770132, NCT00322699, NCT00513539, NCT03727061, NCT00118222, NCT01262716	189, 190
5-ALA (Gliolan)	Porphyrin precursor	Tumor/ mitochondria	Tumor apoptosis	630	**High-grade glioma**, **actinic keratoses**, bladder, esophageal, skin	2017	United States	None	44, 191, 192
MAL (Metvix)	Porphyrin precursor	Tumor/ mitochondria	Tumor apoptosis	630	**Actinic keratoses**, **nonmelanoma skin**	2004	United States, European Union	NCT00473343	193
h-ALA (Hexvix, Cysview)[c]	Porphyrin precursor	Tumor/ mitochondria	Tumor apoptosis	360–450	**Bladder**	2010	United States, European Union	None	194
Verteporfin (Visudyne)	Porphyrin	Tumor/ mitochondria	Tumor apoptosis	690	**Age-related macular degeneration**, pancreatic, breast	2000	United States, Canada, Japan, Russia, China, European Union	NCT03033225, NCT02939274	25, 47, 195

(*Continued*)

Table 2 (*Continued*)

Photosensitizer (brand name)	Chemical family	Localization tissue/cell	Mode of action	Absorption peak (nm)	Cancer type[a]	Year approved	Country	National Clinical Trial no.[b]	Reference(s)
Padeliporfin (TOOKAD)	Bacterio-chlorin	Vasculature/ cell membrane	Vasculature collapse and tumor starvation	753	**Prostate**, renal	2017	European Union	NCT01573156	141
Temoporfin (Foscan)	Chlorin	Tumor and vasculature/ multiorganelle accumulation	Tumor and vasculature apoptosis with potential systemic immune activation	652	**Head and neck**, lung, brain, bile duct, pancreatic, skin	2001	European Union	NCT03003065, NCT01854684	58, 195
Talaporfin (Laserphyrin)	Chlorin	Tumor/ mitochondria	ROS-induced tumor apoptosis	660	**Lung**, liver, colon, brain, esophageal	2004	Japan	NCT00122876, NCT00028405	196, 197
Undergoing clinical trials									
HPPH (Photochlor)	Chlorin	Tumor/ mitochondria and lysosome	ROS-induced tumor apoptosis	665	Head and neck, esophageal, lung	NA	NA	None	64, 65
Fimaporfin[d]	Chlorin	Tumor/ endosome and lysosome	ROS-induced tumor apoptosis	633	Extrahepatic cholangiocarci-noma, colon	NA	NA	NCT04099888	None
Redaporfin	Bacterio-chlorin	Tumor/ Golgi apparatus and ER	ROS-induced tumor apoptosis	750	Advanced head and neck	NA	NA	None	63

[a]Cancer types for which photosensitizer treatment has been clinically approved are in boldface, and those for which photosensitizer treatment is undergoing preclinical trials are in regular typeface.

[b]The National Clinical Trial number is a unique identification code given to each clinical study registered on **https://clinicaltrials.gov/**.

[c]h-ALA compounds are approved for photodynamic diagnostics of bladder cancer and are undergoing clinical trials for bladder cancer PDT.

[d]Fimaporfin is not used as a direct antitumor agent, but is rather used in combination with gemcitabine/cisplatin to induce tumor cell uptake of chemotherapeutics.

Abbreviations: 5-ALA, 5-aminolevulinic acid; ER, endoplasmic reticulum; h-ALA, 5-aminolevulinic acid hexyl ester; HPPH, 2-[1-hexyloxyethyl]-2-devinyl pyropheophorbide-α; MAL, methyl aminolevulinate; NA, not applicable; ROS, reactive oxygen species.

make up Photofrin, the first clinically approved photosensitizing agent. Photofrin was approved by the FDA in 1995 for palliative care of obstructive esophageal and endobronchial non-small-cell lung cancer (37). It is delivered intravenously and rapidly concentrates in the tumor and corresponding vasculature. Endoscope delivery of 630-nm light irradiation is administered to the tumor 48–72 h following intravenous injection. Photofrin accumulates largely in the mitochondria and lysosomes of cells and induces cell death predominantly via apoptosis (38). Photofrin has been widely explored in clinical trials for other cancers such as lung, pancreatic, head and neck, bile duct, brain, gall bladder, and breast. However, inherent problems such as limited penetrance of excitation wavelengths, chemical instability, hydrophobicity-induced aggregation, low in vivo singlet oxygen generation, and offsite accumulation have hindered its diversification into additional cancers and broader establishment as a first-line treatment (39). While Photofrin is still undergoing clinical trials to assess the validity of PDT in a wider range of cancer types, the next generation of PSs are being developed to improve PDT efficacy and selectivity concurrently.

PpIX: protoporphyrin IX

4. SECOND-GENERATION PHOTOSENSITIZERS

Second-generation PSs were designed to improve upon the limitations of the first-generation hematoporphyrins by exhibiting longer wavelength absorption, increased water solubility, and increased tumor-targeting ability. They are based on the general structures of porphyrin precursors, phthalocyanines, chlorins, and bacteriochlorins, with additional side chains to increase solubility. Whereas Photofrin is an oligomeric mix of hematoporphyrins, second-generation PSs, which are all monomeric mixtures, have faster clearance times and improved intratumoral distribution. Below, we discuss current clinically approved second-generation PSs, which are also summarized in **Table 2**.

ALA is the biosynthetic precursor to protoporphyrin IX (PpIX), an endogenous PS used in the synthesis of heme. Photosensitive porphyrins have poor solubility and chemical stability. Use of the water-soluble porphyrin precursor ALA leads to cellular biosynthesis and substantial accumulation of PpIX (40). Cancer cells accumulate higher amounts of PpIX than normal cells do when dosed with ALA, and subsequent photoactivation with 633 nm of light induces ROS and cell death (41). The photodynamic effect is thought to be mediated by mitochondria- and cytoplasm-localized ROS generation in tumor cells and the surrounding vasculature, similar to hematoporphyrins (42). Chemically stable ALA can be delivered topically, as well as orally or intravenously, which has seen great success in localized treatment of precancerous lesions such as actinic keratosis (43). There have been promising clinical trials for bladder cancer: Patients at intermediate or high risk received 50 mL of 8 to 16 mM of hexaminolevulinate (HAL) solution instilled into the bladder following transurethral resection. Following HAL-PDT for 3 months, lesions were absent in 52.9% of patients at 6 months, 23.5% at 9 months, and 11.8% at 21 months (44). Unfortunately, the same results have not been consistently observed with intravenous or oral delivery, which led to offsite accumulation in nerve endings, systemic toxicity, and poor efficacy in clinical trials for prostate cancer (45, 46). This is likely due to variable intratumoral distribution of HAL and oxygen levels, an important diagnostic criterion as discussed above.

Verteporfin is a benzoporphyrin derivative used primarily to treat age-related macular degeneration. It was originally investigated for cancer therapy because of its ability to suppress angiogenesis via vascular destruction, which downregulates genes involved in migration and invasion (47). Verteporfin is rapidly incorporated into plasma low-density lipoprotein (LDL), which allows preferential targeting of cancer and neovascular cells due to increased expression of LDL receptors (48). Once in the tumor microenvironment, verteporfin accumulates intracellularly within the mitochondria, where it induces ROS-mediated apoptosis following 690-nm light irradiation. It has been reported to inhibit growth by interfering with the binding of yes-associated protein (YAP)

and transcriptional coactivator with PDZ-binding motif (TAZ) oncoproteins to the transcriptional enhanced associate domain (TEAD) family of transcription factors, independent of light irradiation (49). Although promising in several in vitro studies, verteporfin does not have significant nonphotoinduced effects in vivo (50–52). However, PDT with verteporfin has shown promise in pancreatic and breast cancers and has moved on to phase II clinical trials (25). Verteporfin is rapidly cleared through the bile, showing decreased photosensitivity and increased penetrance due to the longer wavelength. In the United States, verteporfin is approved for the treatment of macular degeneration and is undergoing clinical trials for the treatment of inoperable pancreatic tumors (NCT03033225) and cutaneous metastases of breast cancer (NCT02939274).

Padeliporfin (TOOKAD) is the third conceptualization of bacteriochlorophylls used for therapeutic PDT. The palladium core of the porphyrin enables greater possibility for excited-state intersystem crossing from the PS's singlet state to the triplet state, which can generate ROS. Padeliporfin has a strong absorbance at 763 nm and accumulates in vasculature-localized prostate tumors while clearing from systemic circulation within a few hours following binding to protein serum albumin (53). In a phase III clinical trial, men with low-risk, localized prostate cancer were given 4 mg/kg of TOOKAD intravenously followed by 753 nm of directed irradiation. At the 24-month follow-up only 28% of men treated with vascular-targeted PDT displayed disease progression, with minimal side effects (54). Following these illuminating results, TOOKAD was approved in the European Union for the treatment of low-risk prostate cancer, and phase I trials have begun for the treatment of obstructing esophagogastric cancer.

Temoporfin (Foscan) is a reduced porphyrin, a chlorin analog with a red-shifted absorbance at 650 nm, which is more intense than that of Photofrin. Isotopically labeled temoporfin is incorporated into serum lipids and localizes in various cellular organelles, excluding the nucleus (55). Upon irradiation, a large number of vacuolization and structural alterations occur to the Golgi apparatus, endoplasmic reticulum (ER), and mitochondria (56). Similar to many PSs, tumor destruction occurs by direct tumor damage as well as vascular damage and the following immune response. Temoporfin was approved in the European Union in 2001 for palliative care of advanced head and neck squamous cell carcinoma (SCC). This was following a phase III clinical trial in which 53% of patients with recurrent/refractory head and neck SCC saw increased quality-of-life benefits (57). Temoporfin has also been investigated as the primary treatment in head and neck, skin, prostate, thoracic, brain, bile duct, breast, and pancreatic cancers (58).

Talaporfin (Laserphyrin) is a mono-L-aspartyl chlorin specifically designed to have lower clearance time than first-generation PSs. It can absorb longer (664 nm) wavelengths compared with first-generation PSs and demonstrates reduced skin photosensitivity (59). Its antitumor effect is mediated primarily by mitochondrial ROS-induced apoptosis, though it localizes in other cytoplasmic organelles, in a manner similar to that described above with verteporfin (60, 61). These improved qualities have led to improved therapeutic outcomes when compared with Photofrin for esophageal cancer (62). It was approved in Japan in 2004 for the treatment of lung cancer and is undergoing clinical trials for the treatment of brain, head and neck, esophagus, liver, and metastatic cancers.

Other second-generation PSs also currently under clinical trials are redaporfin, fimaporfin (NCT04099888), and 2-[1-hexyloxyethyl]-2-devinyl pyropheophorbide-α (HPPH) (63–65). All function through ROS-induced apoptosis. Common drawbacks seen in second-generation PSs are insufficient phototoxicity, poor tumor targeting, and insolubility. Although second-generation PSs are chemically purer than first-generation PSs, self-aggregation has made drug delivery and pharmacokinetic analysis difficult. For example, the tendency of temoporfin to aggregate results in variable clearance times and intratumoral distribution (66). Intravascular aggregation complicates the passive tumor targeting on which second-generation PSs rely for tumor accumulation.

Unfortunately, this method of targeting is often not robust enough to mediate complete tumor destruction. When small-molecule second-generation PSs were designed, the primary focus was on increasing in vitro singlet oxygen generation, as a means to maximize potential tumor phototoxicity, and intracellular localization. This approach has not translated well to clinical models, as passive tumor targeting does not have the level of specificity desired for frontline therapies, and in vitro assessment of singlet oxygen generation does not consider oxygen consumption and intratumoral light scattering (67). Third-generation PSs have focused on tumor targeting, absorption and emission of even longer wavelengths, and improved phototoxicity.

NIR: near infrared

5. THIRD-GENERATION PHOTOSENSITIZERS

Third-generation PSs are currently being designed to improve targeting and advance optical properties including high extinction coefficients, longer wavelength absorbance, and photostability. Wavelengths in the near-infrared (NIR) spectrum (650–1,700 nm) are ideal for in vivo imaging, as they are less absorbed by endogenous biological fluorophores (68). This leads to deeper tissue penetration and improved resolution. The NIR-I window refers to wavelengths from 650 to 900 nm, and NIR-II wavelengths range from 1,000 to 1,700 nm (69).

5.1. Fluorescent Small Molecules

Cyanine dyes, which are fluorescent small molecules that can absorb in the UV, visible, or NIR range, have been widely investigated as PSs for PDT (70, 71). ICG, a disulfonated heptamethine cyanine that absorbs at 780 nm, has been utilized since 1959 for medical diagnostics to track hepatic function, blood flow, and tissue and organ perfusion, and in 2015 its use was expanded to cancer diagnostics. Due to its confinement within the vascular system, ICG's primary use in cancer is for detecting abnormal pulmonary drainage indicative of lymphatic metastasis by SLN mapping (27). Although well characterized, ICG suffers from aggregation, short half-life, poor photostability, nonspecific binding, and poor aqueous stability (72). However, the heptamethine scaffold on which ICG is based is promising for the development of alternative theranostic cyanine dyes. The alkyl side chains are easily conjugated to tumor-targeting moieties, addition of a carbocyclic ring increases the rigidity to improve quantum yields, and *N*-alkyl substitutions can improve phototoxic effects (73). In the past five years, the ability to modify the counterion of promising theranostic cyanine and rhodamine salts has proved useful in increasing the quantum yield (74–77), forming self-assembling nanoparticles, and modulating the passive cytotoxicity without light irradiation (78, 79). Even more compelling, the organic salt formulation has been used to modulate electronic energy levels independent of the bandgap by way of counterion pairing to selectively generate ROS, enabling precise tunability of both cytotoxicity and phototoxicity (80). Several optimized cyanine dyes are currently undergoing preclinical trials to assess therapeutic efficacy capability (30, 81); however, there are many analogs undergoing clinical trials for diagnostics and FGS (82, 83).

NIR-II small molecules are harder to develop due to their need for increased molecular conjugation, instability, and hydrophobicity. In general, achieving light absorption and emission beyond 1,000 nm is a challenging material design problem, as nonradiative rates typically increase substantially when the conjugation is increased to reach bandgaps in this range. This typically results in low quantum yields of less than 1–10% for photoluminescent emission beyond 1,000 nm (84) and would similarly reduce ROS generation yields as well. Although there have been some recent demonstrations with the development of NIR-II dyes (85, 86), more preclinical work has focused on NIR-I dyes with emission tails that extend past 1,000 nm, such as ICG (87). Additional

challenges for NIR-II-based molecules are related to available light sources and imaging cameras with a deep NIR photoresponse, which will need to become more cost-effective and widely available.

5.2. Nanomedicine

Nanostructures exhibit one or more dimensions at the nanometer scale, including atomic, molecular, nanocrystal, and nanoparticle assemblies (88). They can offer specific physicochemical properties; have an increased surface area–to–mass ratio, which alters their reactivity; and possess a great deal of control over particle dimensions (89). They can be grouped on the basis of their class (organic, inorganic, and hybrid), origin (natural or synthetic), ordering (e.g., amorphous nanoparticle versus crystalline nanocrystal versus hierarchical assemblies), and dimensionality (0D, 1D, 2D, and 3D) according to the electron movement along the dimensions in the nanomaterial (90, 91). In the biomedical sciences, nanostructures have shown promise as theranostics, drug carriers, and formulations for drug assembly (92).

Nanoparticles can range from nanometers to several microns in size and can be simple, disordered aggregate ensembles or exhibit hierarchical structures such as with micelles or layered particles. Nanoparticles used as theranostics are primarily organic based, inorganic based, or hybrid composites (93–95). Organic nanoparticles, which can be based on small molecules or polymers, include carbon-based nanostructures (CBNs). CBNs are typically biocompatible, allowing for immune evasion, prolonged blood circulation time, and increased tumor-targeting ability. The most common CBNs used for theranostic purposes, both as direct PSs and as carriers for loading PSs, are graphene, carbon nanotubes, and fullerenes (96). They offer several advantages, including high quantum yield, high stability, and good biocompatibility (97). Although CBNs generally have low toxicity, researchers have raised concerns about their fibrous-like structure (98), which could induce inflammatory and fibrotic reactions, and about mesothelioma or carcinogenic responses in the lining of the lung (99).

Inorganic nanoparticles are predominantly metal (e.g., gold, silver, and aluminum), metal oxides (e.g., titanium oxide, iron oxide, and magnetite), or semiconductors (e.g., silicon, lead sulfide, and cadmium telluride). Inorganic nanoparticles tend to enable more structural control over exact size and shape and the optical resonance can be tuned to NIR regions (100). However, inorganic nanoparticles are typically less biocompatible with cells, leading to poor penetration and superficial ROS generation. They also often have poor absorption coefficients near the bandgap, causing strong absorption of UV and blue wavelengths despite having a NIR bandgap (101). Common examples of inorganic nanoparticles as theranostics are quantum dots, nanorods, and nanoshells.

Quantum dots are luminescent colloidal nanocrystals (or nanoparticles) usually 1–10 nm in size and are composed of semiconductor materials. They have spatial dimensions smaller than the Bohr radius of the bulk excited state, which impart strong quantum confinement effects leading to blue shifts in absorption and emission (102). Nanorods are rod-like 1D nanostructures between 10 and 120 nm (103). Nanorods and nanoshells have a well-established chemistry, and their localized surface plasmon resonance, which comes from the coupling between the electromagnetic field and the collective oscillations of the free conduction electrons at the nanoparticle surface, can efficiently convert the excited-state photon energy to heat (104, 105). They can be made from metallic and nonmetallic elements, such as carbon, gold, and zinc oxide, among many others. The shape of gold nanostructures, such as nanorods and nanoshells, can not only change the absorption and scattering wavelength from visible to the NIR region but also increase their absorption and scattering cross sections, enabling imaging and PTT in this region with deeper optical penetration in biological tissues (106). Gold nanorods, when under irradiation, are also considered

to be excellent imagers for cancer and localizable heat sources, desirable traits in an imaging and PTT nanostructure (107). However, both gold nanorods and gold nanoshells possess a relatively low specific surface area, which limits drug loading and can induce aggregation, blue-shifting the absorption window and decreasing tissue penetration (108).

AIE: aggregation-induced emission

Hybrid nanoparticles for therapy typically rely on multimodal drug treatments, such as combining PDT with O_2 economizers/generators, immune activators, ROS generators, and apoptotic inhibitors. Potential combinatorial therapies are discussed in more detail in Section 10, but nanoparticles offer a clear benefit as a multidrug delivery system. Nanoparticle-mediated PDT allows two antitumor treatments to be combined into one delivery system, improving the synergistic effect compared with independent PSs and chemotherapeutic delivery. This is demonstrated with hybrid nanoparticle C dots, ultrasmall core shell silica nanoparticles, which encapsulate fluorescent molecules and can easily accommodate conjugation of a variety of targeting moieties, notably cyclic (arginine-glycine-aspartic acid-D-tyrosine-lysine) pentapeptide and α-melanocyte-stimulating hormone (109, 110). C dots also undergo radiolabeling with ^{124}I, allowing preoperative positron emission tomography imaging as well as real-time fluorescent imaging. C dots have demonstrated tumor-specific accumulation in a minipig model of spontaneous melanoma, in which micrometastases in lymph nodes have been intraoperatively detected in real time (111). C dots are currently undergoing preliminary clinical trials in patients with melanoma or brain tumors to characterize biodistribution and pharmacokinetics (NCT01266096) as well as SLN mapping (NCT02106598). The clinical relevance of these hybrid-composite nanoparticles is apparent and has the potential to improve surgical diagnostics and therapy. **Table 3** provides examples of nanostructures and their uses in theranostic cancer treatment.

Although nanostructures have proven to be efficient in nanomedicine, a common problem of PSs, especially organic dyes, lies in their high hydrophobicity and rigid planar structures. In particular, when PSs are used in the aggregated state or at high concentrations, the intrinsic fluorescence signals are reduced or disappear because of intermolecular π–π stacking (112). This is well known as the aggregation-caused quenching (ACQ) effect. The formation of aggregates results in diminished imaging quality due to the quenched fluorescence. To minimize the ACQ effect, Luo et al. (113) reported in 2001 that a type of luminogen (i.e., silole derivative) exhibited enhanced fluorescence in the aggregated state, and their finding gave rise to the concept of aggregation-induced emission (AIE). AIE is a photophysical phenomenon in which many organic luminophores show dim or no emission in the dissolved state (single molecular state) but show enhanced emission in the aggregated state because of restricted intramolecular motion (114). AIE nanoparticles present some desirable characteristics, such as excellent photostability, high emission efficiency, and efficient ROS generation in the aggregated state for imaged-guided PDT. In addition, AIE nanoparticles are suitable for in vivo imaging and have deep penetration ability and strong photobleaching resistance. Currently, AIE nanostructures have emerged for various applications, including cancer theranostics, and can occur as different nanostructures, for example, nanodots, nanorods, C dots, and nanosheets (115–118).

6. MODE OF ACTION

PDT induces antitumor effects by three main mechanisms: (*a*) destruction of tumor cells by the generation of ROS, (*b*) collapse of the tumor vasculature and subsequent nutrient starvation of tumor cells, and (*c*) activation of the innate immune system against tumor antigens (**Figure 3**). Different PSs accomplish these mechanisms to varying degrees and being highly efficient at all three is not necessarily needed or desirable. Early destruction of tumor vasculature inhibits the systemic

Table 3 The outcomes and parameters of nanostructured formulations used as theranostics and the potential applications to treat different types of cancer in vitro and in vivo

Class	Structure base	Nanostructure	Role of nanostructure	Nanocomplex structure	Main application(s)	Absorption peak (nm)[a]	Cancer type	Remarks	Reference
Carbon	Graphene	nanoGO sheets	Photothermal and drug delivery agent	Methylene blue–loaded Pluronic F127 coating nanoGO	PDT/PTT	655/808	Cervical cancer (HeLa) in vitro, in vivo	Complete tumor regression with no visible necrotic tissue damage	198
		GQDs	Produce $^1O_2$ with quantum yield greater than 1	UCNP-GQD/TRITC	PDT	980	Breast cancer (4T1) in vitro, in vivo	Mitochondria-specific PDT with in situ $^1O_2$ generation in mitochondria; tumor inhibition efficacy rate 75.3%	81
	Carbon nanotubes	SWCNTs	Photothermal efficacy, improved cargo loading, improved cell penetration, strong Raman signals	Long circulating albumin-Ce6/ECNTs	Imaging/PDT/PTT	630/808	Head and neck carcinoma (SCC-7) in vitro, in vivo	Diagnostic imaging agent for head and neck carcinoma; PTT/PDT together presented complete tumor eradication in vivo	199
	CDs	Aggregation-induced emission nanoparticles	Modulation of morphology and emission of CD intensity	NDI-i-CD-iii[b]	Bioimaging	580	Skin cancer (B16F10 cells) in vitro	Surface-functionalized CDs' emission intensity remarkably enhanced in B16F10 cells	200

(*Continued*)

Table 3 (*Continued*)

Class	Structure base	Nanostructure	Role of nanostructure	Nanocomplex structure	Main application(s)	Absorption peak (nm)[a]	Cancer type	Remarks	Reference
Carbon	Fullerene	C_{60}	ROS production (PDT), heat release (PTT), and improved biocompatibility	C_{60}-IONP-PEG-FA[c]	Imaging, PDT, RTT, and magnetic targeting	532	MCF-7 cells/S180 tumor-bearing BALB/c mice	In vitro and in vivo ROS-triggered apoptosis and displayed potential as an MRI contrast agent	201
Inorganic	Quantum dots	$Cu_2(OH)PO_4$	Improved NIR photoabsorption and ROS production	$Cu_2(OH)PO_4$-@PAA[d]	PDT/PTT/PAT imaging	1,064	Cervical cancer (HeLa cells) in vitro, in vivo	Combinatorial PDT/PTT decreased cell viability by 85% and induced total remission of tumors by photoablation in 80% of mice with IR imaging to monitor therapy	202
	NRs	Metal (e.g., Au) NRs	Photothermal conversion material	Ce6-AuNR@SiO_2-d-CPP[e]	PTT/PDT	650/808	Breast cancer (MCF-7) in vitro, in vivo	Prolonged-circulation; mitochondria targeting decreased cell viability and inhibited tumor growth	203
	NSs	Metal (e.g., Au) NSs	NIR light absorption to form localized heat and improved drug release	BGNSH-HSA-ICG-FA[f]	PTT/PDT/ chemotherapy and imaging	420/808	Breast cancer (MDA-MB-231 cells) in vitro, in vivo	PDT/PTT decreased cell viability by 80% via apoptosis and high-efficiency in vivo fluorescence imaging	204

(*Continued*)

Table 3 (*Continued*)

Class	Structure base	Nanostructure	Role of nanostructure	Nanocomplex structure	Main application(s)	Absorption peak (nm)[a]	Cancer type	Remarks	Reference
Hybrid	NPs	Lipid-encapsulated TPE-PTB	Improved biocompatibility and water dispersity	TPE-PTB	Two-photon imaging/PDT	800	Skin cancer (A375 cells) in vitro, in vivo	Inhibition of tumor growth with no side effects to main organs, potent ROS production ($^1O_2$ and $^{\cdot}OH$); can image deep (up to 505 μm) tumor tissues	205
	NSs	Au-NSs around PLGA	Combination of PTT and fluorescence imaging	Her2-GPH NPs	Imaging/PTT	808	Breast cancer (SKBR3 cells) in vitro	Decreased cell viability by 20% with anti-Her2 antibodies targeting and high-contrast in vitro imaging	206

[a]Experimental groups were exposed to different wavelengths to achieve the effects of the combined therapy (e.g., synergy of PDT/PTT).
[b]Surface-functionalized CDs with L-tyrosine-tagged NDI derivative (NDI-i).
[c]C_{60} loaded with IONPs and functionalized with PEG and FA.
[d]PAA-coated $Cu_2(OH)PO_4$ quantum dots.
[e]Au-NRs coated with the pegylated mesoporous SiO_2 to entrap the PS Ce6 and D-CPP.
[f]PLGA biodegradable matrix loaded with the anticancer drug doxorubicin and covered with a porous Au-NS functionalized with HSA, dye ICG, and FA.
Abbreviations: C_{60}, Buckminsterfullerene; CD, carbon dot; D-CPP, D-type cell-penetrating peptide; ECNT, Evan blue carbon nanotube; FA, folic acid; GPH, gold-nanoshell pegylated magnetic hybrid nanoparticle; GQD, graphene quantum dot; Her2, human epidermal growth factor receptor 2; HSA, human serum albumin; ICG, indocyanine green; IONP, iron oxide nanoparticle; MRI, magnetic resonance imaging; nanoGO, nanographene oxide; NDI, naphthalene diimide derivative; NIR, near-IR; NP, nanoparticle; NR, nanorod; NS, nanoshell; PAA, poly(acrylic acid); PAT, photoacoustic tomography; PDT, photodynamic therapy; PEG, polyethylene glycol; PLGA, poly(lactic-co-glycolic acid); PS, photosensitizer; PTT, photothermal therapy; ROS, reactive oxygen species; RTT, radiofrequency thermal therapy; SCC-7, squamous cell carcinoma-7; SWCNT, single-walled carbon nanotube; TPE-PTB, 4-(5-(1-(4-(*tert*-butyl)phenyl)-1H-phenanthro[9,10d]imidazol-2-yl)-thiophen-2-yl)-7-(4-(1,2,2-triphenylvinyl)phenyl)benzo[c][1,2,5]thiadiazole; TRITC, tetramethyl rhodamine isothiocyanate; UCNP, upconversion nanoparticle.

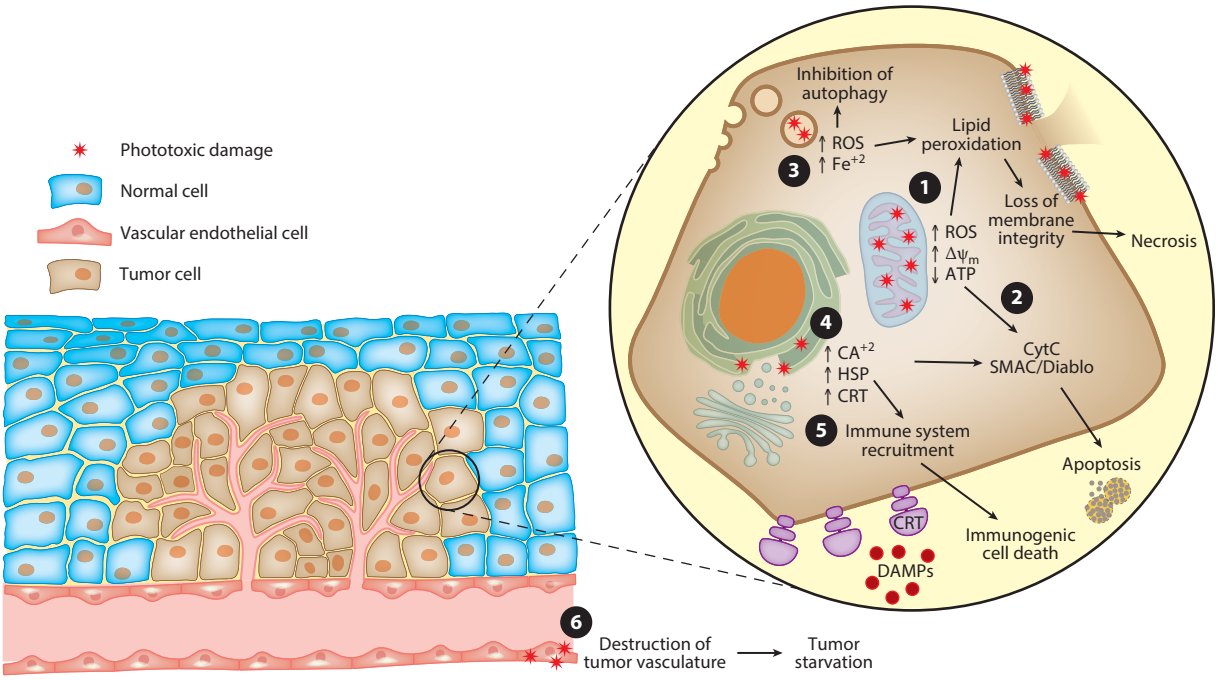

Figure 3

Photodynamic therapy (PDT) induces tumor cell death through various mechanisms depending on photosensitizer (PS) localization. PSs that cause direct tumor cell destruction localize in specific cellular organelles, leading to different cell death pathways. (❶) PSs that localize in the mitochondria generate reactive oxygen species (ROS) and damage the mitochondria, causing a decrease in ATP levels and depolarization of the mitochondrial membrane potential ($\Delta\psi_m$). (❷) This results in the release and recruitment of proapoptotic proteins [cytochrome C (CytC) and the SMAC/Diablo complex] that initiate apoptosis. (❸) PSs that localize in lysosomes also induce ROS while additionally releasing labile iron, which increases cytosolic oxidative damage. Low levels of oxidative damage contribute to apoptosis, and high levels damage membranes to induce necrosis. Furthermore, destruction of lysosomes inhibits autophagy, a mechanism for tumor cell survival. (❹) PSs that photodamage the endoplasmic reticulum release heat shock proteins (HSPs), calcium, and calreticulin (CRT). (❺) High levels of cytosolic calcium trigger apoptosis. HSP release and CRT displays on the cell surface are important damage-associated molecular patterns (DAMPs) that stimulate the antitumor immune system. (❻) PSs that localize within endothelial cells in the tumor vasculature ablate blood vessels and induce tumor starvation.

antitumor immune response and prevents additional drug and oxygen delivery, and highly concentrated ROS generation at the tumor site does not effectively stimulate the innate immune system.

The cell death mechanisms of PSs are influenced by their localization. This can be in the tumor bed, in the tumor vasculature, or directly within the tumor cells. Certain PSs, such as padeliporfin (TOOKAD), have been developed specifically to accumulate in the tumor vasculature and inhibit tumor progression by nutrient starvation (53). This is usually coupled to additional accumulation of PSs in tumor cells. Most second-generation PSs were designed to accumulate within tumor cell organelles to improve tumor destruction. Generation of ROS within mitochondria, Golgi apparatus, ER, and lysosomes can directly initiate apoptosis over a matter of hours. This cleaner form of cell death is thought to be ideal, as the programmed cell death routine releases toxic cellular components in a controlled manner and recognition of the apoptotic marker, phosphatidylserine, by phagocytes suppresses the expression of proinflammatory cytokines (119). Higher doses of light and drug treatment lead to tumor cell necrosis, influenced by nonspecific PS accumulation in the plasma membrane, resulting in immediate catastrophic damage and loss of membrane integrity (38). These necrotic, proinflammatory modes of cell death accelerate tumor growth and metastasis

by recruiting tumor-associated macrophages, which differentiate into growth-/repair-promoting macrophages in the presence of cytokines such as interleukin 6 (IL-6), leukemia inhibitory factor (LIF), tumor necrosis factor (TNF), C-C motif chemokine 22 (CCL-22), and stromal cell-derived factor-12 (CXCL-12) (120, 121). However, certain forms of PDT recruit natural killer and $CD8^+$ cytotoxic T cells to generate an antitumor immune response. Expression of heat shock proteins HSP70 and HSP90, calreticulin, and high mobility group protein B1 (HMBG1) in the presence of ROS-induced damage in the ER stimulates an immunogenic cell death. Expression of these damage-associated molecular patterns (DAMPs) stimulates local inflammatory cells, a necessary mechanism to achieve optimal PDT (122). PDT-stimulated immune response has the acute effect of locally controlling tumor growth and is also preventative against metastasis and tumor recurrence by activating systemic immunosurveillance against tumor cells.

PIT: photoimmunotherapy

Activation of the innate immune system requires adequate blood flow to allow for a systemic antitumor response; thus, PSs designed to ablate tumor vasculature are not ideal. To circumvent this problem, an alternative method combines different intensities of light irradiation, coupling low- and high-fluence-rate light delivery. Fluence rate is the measurement of incident light on a cross-sectional area over a period of time. Initial low-fluence-rate light delivery can induce disperse PDT effects to implement a systemic antitumor immune response, and subsequent high-fluence-rate light delivery can destroy tumor vasculature and lead to acute tumor destruction. The PDT-activated immunogenic cell death response, also called photoimmunotherapy (PIT), was originally observed by the Kobayashi group (123): Light activation of antibody-bound IR700CW leads to a conformational change that irreparably damages the plasma membrane when bound to tumor cell membrane receptors. This damage leads to the release of DAMPs to initiate an immune response. Initially, PIT was found to be independent of ROS generation, instead relying on conformational changes to the antibody structure. However, ICG antibody conjugates also induce a similar effect via direct cellular ROS damage, which has allowed further insight into the molecular mechanisms of antitumor immune system stimulation and into rational design of PSs to induce this effect (124).

7. TARGETING

7.1. Passive Targeting

PDT has traditionally relied on the accumulation of PSs in the tumor site by passive targeting, a phenomenon in which the inherent pathophysiology of tumors allows increased accumulation of macromolecules. This has been exploited primarily in nanomedicine to reduce the side effects associated with many chemotherapeutics by reaching cytotoxic levels of drugs only at the tumor site. Nanoparticles passively accumulate in tumors due to the leaky and malformed vasculature of tumors coupled with poor lymphatic drainage, known as the enhanced permeability and retention (EPR) effect (125). The EPR effect leads to increased accumulation of larger macromolecules and nanoparticles in the tumor bed. Unfortunately, there has been poor clinical translation in human studies due to the heterogeneity of the EPR effect across different types of cancers, individuals, and even tumors and metastases within the same patient (126).

7.2. Active Targeting

Due to the limitations of passive targeting, tumor-specific moieties for active targeting by PSs of tumor tissue have been developed. Tumor-targeting agents include small molecules and antibodies. Small molecules are ideal targeting agents because they are generally inexpensive and do not inhibit cellular uptake of PSs, as sometimes observed with antibodies targeted to membrane

proteins. Conversely, antibodies have a higher degree of tumor selectivity and sensitivity. Simple sugars similar to glucose are popular targeting moieties that have been used for years, most commonly for positron emission tomography scans. Cancer cells overexpress glucose transporter 1 (GLUT-1), which can be manipulated to increase the uptake of conjugated PSs (127, 128). Similar results have been seen with folate, hyaluronic acid, and transferrin (129, 130).

Antibody targeting has the highest degree of specificity for tumor cells (131). Unfortunately, many cancers that require additional therapeutic options do not express easily targetable receptors. Further, large antibodies lead to poor tumor penetration and extended vascular circulation. Antibodies can also induce an immune response and are expensive to synthesize. Smaller antibody fragments can lead to reduced circulation and improved tissue distribution (132). However, smaller antibody fragments require higher-affinity binding to prevent diffusion from the tumor bed and clearance through the vascular system (133).

PDT also has the means to enhance tumor drug uptake and can act as an indirect tumor-targeting technique. Under proper conditions, PDT induces necrotic cell death of tumor cells adjacent to blood vasculature. This perivascular destruction dilates the blood vessel, increasing blood volume but decreasing tumor blood pressure. The combination leads to increased nanoparticle perfusion into the tumor bed (134). This has been studied predominantly with NIR-PIT (near-IR-photoimmunotherapy) using various IR700-antibody conjugations; the PS undergoes ligand dissociation from the antibody's light chain when photoactivated, leading to membrane destruction. However, similar effects in traditional ROS-inducing PSs and upconverting nanoparticles have been seen (135). Histopathology following NIR-PIT shows dilated tumor vasculature with a widened tumor interstitium, which has been confirmed by magnetic resonance imaging and fluorescent visualization of nanoagent accumulation in the tumor bed. This large increase in tumor permeability is known as the super-enhanced permeability and retention (SUPR) effect and has been used to increase tumor accumulation of nanodrug delivery 24-fold (123). The SUPR effect leads to increased targeted uptake of nanomaterials, which offers promising optical properties as well as an ideal platform for multidrug delivery, tumor targeting, and improved biostability.

8. LIGHT DOSING REGIMENS

Fiber optics, light-emitting diodes, and microendoscopic delivery have advanced light delivery to the tumor environment. Clinical trials using interstitial, endoscopic, laparoscopic, and intraoperative light delivery following surgical resection have been performed. However, the inherent heterogeneity of tumors makes standardized regimens of light treatment and drug delivery challenging. Different PSs localize differently within tumors, and tumors have highly varied microenvironments and drug uptake, making it difficult to anticipate the proper light dosimetry to induce a particular effect (136). Higher fluence rates (75 mW/cm^2) rapidly deplete intratumoral oxygen pressure (pO_2) and do not significantly decrease tumor growth as expected (137). Surprisingly, lower fluence rates are more effective for tumor control (137, 138). The rapid generation of ROS with high fluence rates can deplete the tumor oxygen too quickly, creating hypoxic conditions that inhibit PDT and promote tumor cell survival. Premature vascular collapse also inhibits local tumor phototoxicity, blocking the delivery of additional O_2 and PSs. Studies have found that an initial low-fluence-rate light delivery, followed by high-fluence-rate light delivery, improves the efficacy of PDT using the clinically approved PS agent temoporfin (139). Administering two independent light treatments with differing dosimetries improves antitumor efficacy in several models and across multiple PSs (140). Monitoring tumor oxygen levels during PDT may enable real-time adjustments to light distribution and intensity, as different PSs can consume oxygen at different rates (141, 142). Timing of light treatment is complicated by PS pharmacokinetics, which varies

dramatically between PSs, and an optimal light treatment window can vary from hours to days after PS delivery. A major limitation to PDT is recurrence, which is thought to occur due to incomplete tumor response to therapy. Optimizing light treatment regimens based on the mode of action of a specific PS would reduce recurrence and improve outcomes.

9. RESISTANCE MECHANISMS

Autophagy, the degradation and recycling of cellular components, promotes cell survival under harsh conditions and is often upregulated in cancer cells that are resistant to traditional radiotherapies and chemotherapies. Increased expression of autophagy markers in cancer stem cells and malignant precursor cells has been reported (143, 144). Autophagy can decrease the efficacy of mitochondria-targeted PDT, and incomplete tumor response following PDT increases expression of autophagy proteins in tumor cells (145, 146). To address this, researchers have used combinatorial therapy with autophagy-inhibiting agents to sensitize cells to PDT (147). PDT in combination with lysosome- and mitochondria-targeting PSs should also be considered to avoid autophagy-induced resistance; lysosomal destruction halts the recycling of biomolecules that promote cancer cell survival via autophagy mechanisms. For example, the combination of two PSs, phenylbenzothiazole (EtNBS) and verteporfin, showed a 95% reduction in the weights of fibrosarcomas in BALB/c mice (148). This level of advanced photokilling could not be replicated with dramatically higher doses of either PS administered alone or with higher doses of light treatment. These two agents localize to different organelles within the cell: EtNBS localizes to the lysosomes, inhibiting apoptosis and releasing labile iron and Ca^{+2}; verteporfin localizes primarily to mitochondria and the ER to induce apoptosis. Although more preclinical data are needed, combining PDT with autophagy or lysosome inhibitors could increase efficacy for large tumor debulking or complete tumor response. Understanding the distinct mode of action of specific PSs is important for developing combinatorial treatments that inhibit cell survival programs induced by PDT.

The destructive effect of PDT relies primarily on the production of ROS, which causes irreversible oxidative damage to membranes and organelles. Unfortunately, cancer cells tend to have highly dynamic stress resistance mechanisms, including high levels of superoxide dismutases (SODs), glutathione peroxidase, and thioredoxins (149). This promotes a highly oxidative environment, promoting genetic instability and increased resistance to cell death mechanisms. Following PDT, MDA-MB-231 breast cancer cell xenografts show an immediate increase in inducible nitric oxide synthase (iNOS) and nitric oxide, which leads to increased tumor growth and inhibition of ROS-induced apoptosis (150). Administration of NOS inhibitors improves PDT efficacy with Photofrin, likely by hindering the cytoprotective effects of iNOS (151, 152), though these benefits are observed only with high-fluence-rate PDT (153).

Resistance to apoptosis is a hallmark of cancer and has been well reported for PDT (145, 154). Overexpression of antiapoptotic *Bcl-2* and underexpression of proapoptotic *Bid* and *Bax* inhibit cell death programs to improve cell survival during PDT (155). Low-power PDT leads to increases in the survival and stress responses, as upregulation is seen in hypoxia inducible factor 1 (HIF-1)- and nuclear factor–κB (NF-κB)-induced genes (156). Because failure of PDT to fully eradicate tumors can lead to increased malignancy and tumor progression, treatment regimens must be appropriately designed to avoid inadvertently triggering protumor cell programs.

Increased expression of drug efflux pumps is a well-established mode of drug resistance. This remains true for PDT, though the efflux pumps expressed tend to correlate to the localization and mode of uptake of the PS. ATP-binding cassette super-family G member 2 (ABCG2) is an efflux pump commonly expressed in multidrug-resistant cancers, and several PSs are known substrates (157). Increased expression is seen after low-dose PDT, and upregulation in cell lines reduces

the efficiency of PDT (155). Inhibition of efflux pumps has been successful in antibacterial PDT: Treatment with methylene blue PDT is improved when it is combined with a microbial efflux pump inhibitor (158). Additionally, cell lines resistant to mitochondrial PDT show changes to mitochondrial structure and metabolism, though more research is needed to determine the exact molecular mechanisms (159, 160). Overall, this is an area where more research is needed in order to interpret potential resistances associated with therapy and improved indicators for cancers where PDT could be an ideal therapeutic option.

10. COMBINATORIAL THERAPY

Increased knowledge about the biochemical interactions driving tumor progression has led to combinatorial treatment, by which multiple pathways are targeted to improve response to therapy and mitigate drug resistance (161). PDT already has the benefit of targeting multiple cell death pathways by inducing direct damage to mitochondria, Golgi apparatus, ER, and lysosomes, creating widespread irreversible cell damage at proper dosages. As discussed above, combining PDT with autophagy or lysosome inhibitors may be effective against tumors with high levels of autophagy. The combinatorial therapies discussed below focus on targeting additional pathways to enhance PDT and subvert tumor survival responses.

10.1. Impairment of Cellular Redox

Many combinatorial treatments enhance the primary mechanism of PDT—generation of ROS. PDT can be augmented by increasing tumor oxygen saturation, interfering with cellular redox balance, or potentiating the effects of PDT-generated ROS. Antioxidant inhibitors have had poor effects independently but show promise for enhancing the effects of PDT (162, 163). Dysfunction to redox homeostasis via cellular antioxidant inhibitors such as diethyldithiocarbamate (a Cu/Zn-SOD inhibitor), 2-methoxyestradiol (a Mn-SOD inhibitor), L-buthionine sulfoximine (a glutathione synthesis inhibitor), and 3-amino-1,2,4-triazole (a catalase inhibitor) has displayed increased cell death and ROS generation with traditional PDT agents in cell models but requires further study in animal models (163). Exogenous small-molecule antioxidants such as vitamins E (tocopherol) and C (ascorbate) have shown promise both as protective agents in normal cells and as selectively toxic agents against cancer cells at higher pro-oxidant concentrations (164). However, reaching clinically effective dosages of these agents has proved to be difficult, which has limited their use and study. Hollow MnO_2 nanoparticles have become a promising nanoplatform for PDT, as they provide delivery of PSs, which tend to be poorly soluble, and also stimulate oxygen levels. MnO_2 catalyzes the breakdown of H_2O_2 into water and oxygen, maintaining stable levels of oxygen for a prolonged PDT response (165, 166). MnO_2 nanosheets have also been implemented with PDT to oxidize intracellular glutathione, which impairs the antioxidant response to ROS generation (167). There have been many studies of the antineoplastic effects of cannabidiol, which increase ROS generation in mitochondria and ER of cancer cells (168). Although not efficacious on its own, cannabidiol showed dramatically increased potency when combined with PDT and radiotherapy (169). For ALA prodrugs, agents that alter heme and iron metabolism have led to increased accumulation of PpIX and subsequent improvements to PDT in preclinical models (170–172).

10.2. Ferroptosis

Ferroptosis is another form of regulated cell death that ties in closely with oxidative stress and cancer. This unique form of cell death is based on iron-dependent lipid peroxidation. Cellular iron

homeostasis is highly regulated due to the high reactivity of labile iron with oxygen to form ROS (173). Ferroptosis can be induced by perturbations to the glutathione antioxidant network and metabolism, inhibition of glutathione peroxidase 4 (GPX4), and increasing levels of intracellular iron. For example, although pancreatic cancer is highly resistant to cellular apoptotic mechanisms, ferroptosis can subvert typical apoptotic cell signaling to induce cell death in pancreatic ductal adenocarcinoma cell lines (174, 175). Iron chelators such as deferoxamine combined with prodrug ALA treatment have been investigated, as the sequestration of iron inhibits the final step of heme synthesis, increasing the generation of photoactive PpIX from ALA (176, 177). Conversely, iron chelation can also inhibit ferroptosis; iron complexed with deferoxamine lacks redox potency, reducing the efficacy of PDT-induced cell death (178). Potential PDT combinatorial methods could involve dual delivery of small-molecule ferroptosis inducers (e.g., erastin, sorafenib, and RSL3), iron doping via nanoparticle delivery, and iron-based nanoparticles. Not only has ferroptosis been shown to resensitize cancer cells to chemotherapy and promote PDT, but high levels of ROS combined with labile iron could produce O_2 via Fenton reactions. This would resupply the hypoxic tumor microenvironment with molecular oxygen, solving a key problem inherent to PDT. Finally, many ferroptosis inducers act by inhibiting the cellular redox balance, a mechanism that would also enhance PDT.

10.3. Tumor Sensitization

PDT has been shown to improve the outcome of traditional chemotherapy and radiotherapy. Although PDT itself primarily has a localized effect, resulting in minimal side effects, it can also heighten the effect of radiotherapies and chemotherapies. Sensitization of the tumor to traditional therapies allows for lower effective doses, reducing side effects while improving therapeutic outcomes. This has been especially notable with platinum-based chemotherapeutics because of their induced expression of proapoptotic pathway proteins (179). In xenograft models of small-cell lung cancer, low-dose cisplatin combined with PDT displayed a synergistic effect on tumor size when compared with either treatment alone (180). However, reports regarding cisplatin in preclinical models have been contradictory; due to the reliance of PDT efficacy on the immune system, nude mouse models may not be appropriate for this type of therapy (181). PDT combined with radiotherapy led to similar results, although the interaction between the two treatments has proved difficult to study. The combination of verteporfin and radiation therapy showed a 60% reduction in tumor doubling time in patients with fibrosarcoma (182). Reduced side effects are common with this type of combinatorial therapy, but the mechanism for the unexpectedly low cross-interaction toxicity has yet to be determined (183).

10.4. Immunostimulators

Immune activation is a crucial part of the PDT mechanism. An increased immune response has been reported to promote PDT efficacy in human patients, provoking interest in enhancing this effect (184). Immune checkpoint therapy in T cells enhances antitumor therapy by preventing tumor proteins from inhibiting the activation response of T effector cells (185). Treatment of bilateral cancer in cholinergic mouse models with a pyrolipid PS and PD-1/PD-L1 (programmed cell death protein 1/programmed cell death ligand 1) axis inhibitor (oxaliplatin) improved regression of the primary-site, light-treated tumor as well as that of distant tumors. This abscopal effect was attributed to antitumor immunity, evidenced by increased exposure to calreticulin by treated tumor cells followed by increased presence of $CD8^+$ and $CD4^+$ T cells at distant tumor sites (186). Similar synergistic effects have been observed with immunostimulators, such as glycated

chitosan, CpG oligodeoxynucleotides, and cyclophosphamide, as well as other immune checkpoint inhibitors (187, 188).

11. CONCLUSIONS AND FUTURE OUTLOOK

In this review, we have highlighted the scientific advances in photoactive theranostics that are expanding clinical PDT and photodynamic diagnostic applications. These advances have the potential to revolutionize modern treatments of cancer and other diseases. Breakthroughs in materials science, electronics, and imaging equipment have enabled exploration into NIR fluorophores/phosphors and have expanded the clinical applicability of PDT. This expansion has facilitated novel investigations into photosensitizing agents in order to meet the demand for optimized, accessible cancer treatments. We have summarized several innovative and promising preclinical works. Moving these multimodal PSs into clinical settings should be prioritized. However, several areas still need to be advanced in order to fully realize the tremendous potential of photoactive theranostics. The wide variety of PSs studied with different tumor and cellular models has made it difficult to develop optimized regimens for ideal patient outcomes. Further research into each potential theranostic agent is needed to determine proper dosing criteria, both for the photoactive agent and for the activating light. Improved PS agents need to be designed with minimal off-target effects, greater selectivity, enhanced phototoxicity, and enhanced penetrance. Additional standards, generally neglected in the literature, are required to establish proper dosing intervals for different combinatorial therapies with PDT. Whether PDT is being used as a sensitizing agent, an immune activator, or the primary treatment, it will have different dosing windows depending on the combined therapy. Substandard clinical trial results may be due to variable pharmacokinetics, which is important for determining the timing of light treatment. Furthermore, PDT is an ideal complement for combinatorial therapies with great potential for enhancing tumor-killing efficacy beyond that of either approach alone and for enabling greater space for treatment development and exploration. Many of the chemotherapeutic agents discussed are well tolerated at low concentrations, and the combination of tumor targeting and broad effects of PDT promises a potent antitumor effect. Future work should aim to improve the efficacy of PDT through rationally designed treatment strategies, to explore novel photoactive materials, and to continue to expand applications in a broader range of cancer types.

DISCLOSURE STATEMENT

This review is based on work supported by the National Science Foundation under CAREER grant no. CBET 1845006 to S.Y.L., the National Science Foundation under grant no. CBET 1702591 to R.R.L., and a Michigan State University Strategic Partnership Grant.

ACKNOWLEDGMENTS

The authors thank Matthew Bates, Elliot Ensink, and Shao Thing Teoh for helpful discussions and a critical reading of the manuscript. For image elements used in the figures, we acknowledge somersault18:24 (**http://www.somersault1824.com/**) (CC BY-NC-SA 4.0).

LITERATURE CITED

1. Huang H, Song W, Rieffel J, Lovell JF. 2015. Emerging applications of porphyrins in photomedicine. *Front. Phys.* 3:23

2. Cheng L, Wang C, Feng L, Yang K, Liu Z. 2014. Functional nanomaterials for phototherapies of cancer. *Chem. Rev.* 114(21):10869–939
3. Li Y, Lin T, Luo Y, Liu Q, Xiao W, et al. 2014. A smart and versatile theranostic nanomedicine platform based on nanoporphyrin. *Nat. Commun.* 5(1):4712
4. Patel SK, Janjic JM. 2015. Macrophage targeted theranostics as personalized nanomedicine strategies for inflammatory diseases. *Theranostics* 5(2):150–72
5. Pushpan S, Venkatraman S, Anand V, Sankar J, Parmeswaran D, et al. 2002. Porphyrins in photodynamic therapy—a search for ideal photosensitizers. *Curr. Med. Chem. Anticancer Agents* 2(2):187–207
6. Oniszczuk A, Wojtunik-Kulesza KA, Oniszczuk T, Kasprzak K. 2016. The potential of photodynamic therapy (PDT)—experimental investigations and clinical use. *Biomed. Pharmacother.* 83:912–29
7. Hönigsmann H. 2013. History of phototherapy in dermatology. *Photochem. Photobiol. Sci.* 12(1):16–21
8. Calixto G, Bernegossi J, de Freitas L, Fontana C, Chorilli M. 2016. Nanotechnology-based drug delivery systems for photodynamic therapy of cancer: a review. *Molecules* 21(3):342
9. Liu Y, Bhattarai P, Dai Z, Chen X. 2019. Photothermal therapy and photoacoustic imaging via nanotheranostics in fighting cancer. *Chem. Soc. Rev.* 48(7):2053–108
10. Foote CS. 1991. Definition of type I and type II photosensitized oxidation. *Photochem. Photobiol.* 54(5):659
11. Lan G, Ni K, Lin W. 2019. Nanoscale metal-organic frameworks for phototherapy of cancer. *Coord. Chem. Rev.* 379:65–81
12. Celli JP, Spring BQ, Rizvi I, Evans CL, Samkoe KS, et al. 2010. Imaging and photodynamic therapy: mechanisms, monitoring, and optimization. *Chem. Rev.* 110(5):2795–838
13. Morton CA, Szeimies R-M, Basset-Séguin N, Calzavara-Pinton PG, Gilaberte Y, et al. 2020. European Dermatology Forum guidelines on topical photodynamic therapy 2019 Part 2: emerging indications - field cancerization, photorejuvenation and inflammatory/infective dermatoses. *J. Eur. Acad. Dermatol. Venereol.* 34(1):17–29
14. Raab O. 1900. On the effect of fluorescent substances on infusoria. *Z. Biol.* 39:524–26
15. Macmillan JD, Maxwell WA, Chichester CO. 1966. Lethal photosensitization of microorganisms with light from a continuous-wave gas laser. *Photochem. Photobiol.* 5(7):555–65
16. Taub AF. 2007. Photodynamic therapy: other uses. *Dermatol. Clin.* 25(1):101–9
17. Hamblin MR, Hasan T. 2004. Photodynamic therapy: a new antimicrobial approach to infectious disease? *Photochem. Photobiol. Sci.* 3(5):436–50
18. Araújo NC, Fontana CR, Bagnato VS, Gerbi MEM. 2014. Photodynamic antimicrobial therapy of curcumin in biofilms and carious dentine. *Lasers Med. Sci.* 29(2):629–35
19. Hu Z, Liu L, Zhang W, Liu H, Li J, et al. 2018. Dynamics of HPV viral loads reflect the treatment effect of photodynamic therapy in genital warts. *Photodiagn. Photodyn. Ther.* 21:86–90
20. Wainwright M. 2004. Photoinactivation of viruses. *Photochem. Photobiol. Sci.* 3(5):406–11
21. van Straten D, Mashayekhi V, de Bruijn HS, Oliveira S, Robinson DJ. 2017. Oncologic photodynamic therapy: basic principles, current clinical status and future directions. *Cancers* 9(2):19
22. Mimura S, Ito Y, Nagayo T, Ichii M, Kato H, et al. 1996. Cooperative clinical trial of photodynamic therapy with Photofrin II and excimer dye laser for early gastric cancer. *Lasers Surg. Med.* 19(2):168–72
23. Golusiński P, Szybiak B, Wegner A, Pazdrowski J, Pieńkowski P. 2015. Photodynamic therapy in palliative treatment of head and neck cancer. *Otolaryngol. Pol.* 69(3):15–20
24. Hamblin MR. 2020. Photodynamic therapy for cancer: What's past is prologue. *Photochem. Photobiol.* 96(3):506–16
25. Isakoff SJ, Rogers GS, Hill S, McMullan P, Habin KR, et al. 2017. An open label, phase II trial of continuous low-irradiance photodynamic therapy (CLIPT) using verteporfin for the treatment of cutaneous breast cancer metastases. *J. Clin. Oncol.* 35:TPS1121
26. Mery E, Golzio M, Guillermet S, Lanore D, Le Naour A, et al. 2017. Fluorescence-guided surgery for cancer patients: a proof of concept study on human xenografts in mice and spontaneous tumors in pets. *Oncotarget* 8(65):109559–74
27. Jewell EL, Huang JJ, Abu-Rustum NR, Gardner GJ, Brown CL, et al. 2014. Detection of sentinel lymph nodes in minimally invasive surgery using indocyanine green and near-infrared fluorescence imaging for uterine and cervical malignancies. *Gynecol. Oncol.* 133:274–77

28. Cho SS, Salinas R, Lee JYK. 2019. Indocyanine-green for fluorescence-guided surgery of brain tumors: evidence, techniques, and practical experience. *Front. Surg.* 6:11
29. Kim SH, Rho SY, Kang CM. 2018. Indocyanine green-fluorescent pancreatic perfusion-guided resection of distal pancreas in solid pseudopapillary neoplasm: usefulness and feasibility during pancreaticobiliary surgery. *J. Minim. Invasive Surg.* 21(1):43–45
30. Zhang C, Zhao Y, Zhang H, Chen X, Zhao N, et al. 2017. The application of heptamethine cyanine dye DZ-1 and indocyanine green for imaging and targeting in xenograft models of hepatocellular carcinoma. *Int. J. Mol. Sci.* 18(6):1332
31. Stummer W, Pichlmeier U, Meinel T, Wiestler OD, Zanella F, et al. 2006. Fluorescence-guided surgery with 5-aminolevulinic acid for resection of malignant glioma: a randomised controlled multicentre phase III trial. *Lancet Oncol.* 7(5):392–401
32. Hadjipanayis CG, Stummer W. 2019. 5-ALA and FDA approval for glioma surgery. *J. Neurooncol.* 141(3):479–86
33. Lwin TM, Murakami T, Miyake K, Yazaki PJ, Shivley JE, et al. 2018. Tumor-specific labeling of pancreatic cancer using a humanized anti-CEA antibody conjugated to a near-infrared fluorophore. *Ann. Surg. Oncol.* 25(4):1079–85
34. Tummers WS, Miller SE, Teraphongphom NT, Gomez A, Steinberg I, et al. 2018. Intraoperative pancreatic cancer detection using tumor-specific multimodality molecular imaging. *Ann. Surg. Oncol.* 25(7):1880–88
35. Arsen'ev AI, Kanaev SV, Barchuk AS, Vedenin IO, Klitenko VN, et al. 2007. Опыт эндотрахеобронхиальных операций в комбинации с химиолучевыми методами при лечении распространенного немелкоклегочного рака легкого [Use of endotracheobronchial surgery in conjunction with radiochemotherapy for advanced non-small lung cancer]. *Vopr. Onkol.* 53(4):461–67
36. Simone CB 2nd, Cengel KA. 2014. Photodynamic therapy for lung cancer and malignant pleural mesothelioma. *Semin. Oncol.* 41(6):820–30
37. Higa JT, Hwang JH. 2016. History of ablative therapies for Barrett's and superficial adenocarcinoma. In *Barrett's Esophagus: Emerging Evidence for Improved Clinical Practice*, ed. DK Pleskow, T Erim, pp. 133–49. Boston: Academic
38. Hsieh Y-J, Wu C-C, Chang C-J, Yu J-S. 2003. Subcellular localization of Photofrin determines the death phenotype of human epidermoid carcinoma A431 cells triggered by photodynamic therapy: When plasma membranes are the main targets. *J. Cell. Physiol.* 194(3):363–75
39. Dougherty TJ, Cooper MT, Mang TS. 1990. Cutaneous phototoxic occurrences in patients receiving Photofrin®. *Lasers Surg. Med.* 10:485–88
40. Sachar M, Anderson KE, Ma X. 2016. Protoporphyrin IX: the good, the bad, and the ugly. *J. Pharmacol. Exp. Ther.* 356(2):267–75
41. Fukuda H, Paredes S, Batlle AM. 1989. Tumor-localizing properties of porphyrins. In vitro studies using the porphyrin precursor, aminolevulinic acid, in free and liposome encapsulated forms. *Drug Des. Deliv.* 5(2):133–39
42. Chen R, Huang Z, Chen G, Li Y, Chen X, et al. 2008. Kinetics and subcellular localization of 5-ALA-induced PpIX in DHL cells via two-photon excitation fluorescence microscopy. *Int. J. Oncol.* 32(4):861–67
43. de Oliveira ER, Inada NM, Blanco KC, Bagnato VS, Salvio AG. 2019. Cancerization field treatment using topical photodynamic therapy: a comparison between two aminolevulinate derivatives. *Photodiagn. Photodyn. Ther.* 30:101603
44. Berger AP, Steiner H, Stenzl A, Akkad T, Bartsch G, Holtl L. 2003. Photodynamic therapy with intravesical instillation of 5-aminolevulinic acid for patients with recurrent superficial bladder cancer: a single-center study. *Urology* 61(2):338–41
45. Inoue K. 2017. 5-Aminolevulinic acid-mediated photodynamic therapy for bladder cancer. *Int. J. Urol.* 24(2):97–101
46. Warren CB, Karai LJ, Vidimos A, Maytin EV. 2009. Pain associated with aminolevulinic acid-photodynamic therapy of skin disease. *J. Am. Acad. Dermatol.* 61(6):1033–43
47. Kang M-H, Jeong GS, Smoot DT, Ashktorab H, Hwang CM, et al. 2017. Verteporfin inhibits gastric cancer cell growth by suppressing adhesion molecule FAT1. *Oncotarget* 8(58):98887–97

48. Aquaron R, Forzano O, Murati JL, Fayet G, Aquaron C, Ridings B. 2002. Simple, reliable and fast spectrofluorometric method for determination of plasma verteporfin (Visudyne) levels during photodynamic therapy for choroidal neovascularization. *Cell. Mol. Biol.* 48(8):925–30
49. Scott LJ, Goa KL. 2000. Verteporfin. *Drugs Aging* 16(2):139–46
50. Gibault F, Corvaisier M, Bailly F, Huet G, Melnyk P, Cotelle P. 2016. Non-photoinduced biological properties of verteporfin. *Curr. Med. Chem.* 23(11):1171–84
51. Lui JW, Xiao S, Ogomori K, Hammarstedt JE, Little EC, Lang D. 2019. The efficiency of verteporfin as a therapeutic option in pre-clinical models of melanoma. *J. Cancer* 10(1):1–10
52. Wei H, Wang F, Wang Y, Li T, Xiu P, et al. 2017. Verteporfin suppresses cell survival, angiogenesis and vasculogenic mimicry of pancreatic ductal adenocarcinoma via disrupting the YAP-TEAD complex. *Cancer Sci.* 108(3):478–87
53. Mazor O, Brandis A, Plaks V, Neumark E, Rosenbach-Belkin V, et al. 2005. WST11, a novel water-soluble bacteriochlorophyll derivative; cellular uptake, pharmacokinetics, biodistribution and vascular-targeted photodynamic activity using melanoma tumors as a model. *Photochem. Photobiol.* 81(2):342–51
54. Azzouzi A-R, Vincendeau S, Barret E, Cicco A, Kleinclauss F, et al. 2017. Padeliporfin vascular-targeted photodynamic therapy versus active surveillance in men with low-risk prostate cancer (CLIN1001 PCM301): an open-label, phase 3, randomised controlled trial. *Lancet Oncol.* 18(2):181–91
55. Michael-Titus AT, Whelpton R, Yaqub Z. 1995. Binding of temoporfin to the lipoprotein fractions of human serum. *Br. J. Clin. Pharmacol.* 40(6):594–97
56. Teiten M-H, Marchal S, D'Hallewin MA, Guillemin F, Bezdetnaya L. 2003. Primary photodamage sites and mitochondrial events after Foscan photosensitization of MCF-7 human breast cancer cells. *Photochem. Photobiol.* 78(1):9–14
57. D'Cruz AK, Robinson MH, Biel MA. 2004. mTHPC-mediated photodynamic therapy in patients with advanced, incurable head and neck cancer: a multicenter study of 128 patients. *Head Neck* 26(3):232–40
58. Senge MO, Brandt JC. 2011. Temoporfin (Foscan®, 5,10,15,20-tetra(*m*-hydroxyphenyl)chlorin)—a second-generation photosensitizer. *Photochem. Photobiol.* 87(6):1240–96
59. Tsukagoshi S, Tokyo Cooperative Oncology Group. 2004. 光線力学的治療法に用いる新しい光感受性物質 talaporfin sodium についxて [Development of a novel photosensitizer, talaporfin sodium, for the photodynamic therapy (PDT)]. *Gan To Kagaku Ryoho* 31(6):979–85
60. Kanda T, Sugihara T, Takata T, Mae Y, Kinoshita H, et al. 2019. Low–density lipoprotein receptor expression is involved in the beneficial effect of photodynamic therapy using talaporfin sodium on gastric cancer cells. *Oncol. Lett.* 17(3):3261–66
61. Miki Y, Akimoto J, Yokoyama S, Homma T, Tsutsumi M, et al. 2013. Photodynamic therapy in combination with talaporfin sodium induces mitochondrial apoptotic cell death accompanied with necrosis in glioma cells. *Biol. Pharm. Bull.* 36(2):215–21
62. Ohashi S, Kikuchi O, Tsurumaki M, Nakai Y, Kasai H, et al. 2014. Preclinical validation of talaporfin sodium-mediated photodynamic therapy for esophageal squamous cell carcinoma. *PLOS ONE* 9(8):e103126
63. Oliveira J, Monteiro E, Santos J, Silva JD, Almeida L, Santos LL. 2017. A first in human study using photodynamic therapy with Redaporfin in advanced head and neck cancer. *J. Clin. Oncol.* 35(15 Suppl.):e14056
64. Nava HR, Allamaneni SS, Dougherty TJ, Cooper MT, Tan W, et al. 2011. Photodynamic therapy (PDT) using HPPH for the treatment of precancerous lesions associated with Barrett's esophagus. *Lasers Surg. Med.* 43(7):705–12
65. Rigual NR, Shafirstein G, Frustino J, Seshadri M, Cooper M, et al. 2013. Adjuvant intraoperative photodynamic therapy in head and neck cancer. *JAMA Otolaryngol. Head Neck Surg.* 139(7):706–11
66. Jones HJ, Vernon DI, Brown SB. 2003. Photodynamic therapy effect of m-THPC (Foscan®) in vivo: correlation with pharmacokinetics. *Br. J. Cancer* 89(2):398–404
67. Li B, Lin L, Lin H, Wilson BC. 2016. Photosensitized singlet oxygen generation and detection: recent advances and future perspectives in cancer photodynamic therapy. *J. Biophotonics* 9(11–12):1314–25
68. Kosaka N, Ogawa M, Choyke PL, Kobayashi H. 2009. Clinical implications of near-infrared fluorescence imaging in cancer. *Future Oncol.* 5(9):1501–11

69. Cao J, Zhu B, Zheng K, He S, Meng L, et al. 2020. Recent progress in NIR-II contrast agent for biological imaging. *Front. Bioeng. Biotechnol.* 7:487
70. Haque A, Faizi MSH, Rather JA, Khan MS. 2017. Next generation NIR fluorophores for tumor imaging and fluorescence-guided surgery: a review. *Bioorg. Med. Chem.* 25(7):2017–34
71. Hong G, Antaris AL, Dai H. 2017. Near-infrared fluorophores for biomedical imaging. *Nat. Biomed. Eng.* 1:0010
72. Wang H, Li X, Tse BW-C, Yang H, Thorling CA, et al. 2018. Indocyanine green-incorporating nanoparticles for cancer theranostics. *Theranostics* 8(5):1227–42
73. Usama SM, Thavornpradit S, Burgess K. 2018. Optimized heptamethine cyanines for photodynamic therapy. *ACS Appl. Bio Mater.* 1(4):1195–205
74. Kilin VN, Anton H, Anton N, Steed E, Vermot J, et al. 2014. Counterion-enhanced cyanine dye loading into lipid nano-droplets for single-particle tracking in zebrafish. *Biomaterials* 35(18):4950–57
75. Shulov I, Arntz Y, Mély Y, Pivovarenko VG, Klymchenko AS. 2016. Non-coordinating anions assemble cyanine amphiphiles into ultra-small fluorescent nanoparticles. *Chem. Commun.* 52(51):7962–65
76. Reisch A, Didier P, Richert L, Oncul S, Arntz Y, et al. 2014. Collective fluorescence switching of counterion-assembled dyes in polymer nanoparticles. *Nat. Commun.* 5(1):4089
77. Shulov I, Oncul S, Reisch A, Arntz Y, Collot M, et al. 2015. Fluorinated counterion-enhanced emission of rhodamine aggregates: ultrabright nanoparticles for bioimaging and light-harvesting. *Nanoscale* 7(43):18198–210
78. Magut PKS, Das S, Fernand VE, Losso J, McDonough K, et al. 2013. Tunable cytotoxicity of rhodamine 6G via anion variations. *J. Am. Chem. Soc.* 135(42):15873–79
79. Siraj N, Kolic PE, Regmi BP, Warner IM. 2015. Strategy for tuning the photophysical properties of photosensitizers for use in photodynamic therapy. *Chemistry* 21(41):14440–46
80. Broadwater D, Bates M, Jayaram M, Young M, He J, et al. 2019. Modulating cellular cytotoxicity and phototoxicity of fluorescent organic salts through counterion pairing. *Sci. Rep.* 9(1):15288
81. Zhang C, Zhao Y, Zhao N, Tan D, Zhang H, et al. 2018. NIRF optical/PET dual-modal imaging of hepatocellular carcinoma using heptamethine carbocyanine dye. *Contrast Media Mol. Imaging* 2018:4979746
82. Randall LM, Wenham RM, Low PS, Dowdy SC, Tanyi JL. 2019. A phase II, multicenter, open-label trial of OTL38 injection for the intra-operative imaging of folate receptor-alpha positive ovarian cancer. *Gynecol. Oncol.* 155(1):63–68
83. Lamberts LE, Koch M, de Jong JS, Adams ALL, Glatz J, et al. 2017. Tumor-specific uptake of fluorescent bevacizumab-IRDye800CW microdosing in patients with primary breast cancer: a phase I feasibility study. *Clin. Cancer Res.* 23(11):2730–41
84. Li D, Qu C, Liu Q, Wu Y, Hu X, et al. 2020. Monitoring the real-time circulatory system-related physiological and pathological processes in vivo using a multifunctional NIR-II probe. *Adv. Funct. Mater.* 30(6):1906343
85. Antaris AL, Chen H, Cheng K, Sun Y, Hong G, et al. 2016. A small-molecule dye for NIR-II imaging. *Nat. Mater.* 15(2):235–42
86. Wang S, Fan Y, Li D, Sun C, Lei Z, et al. 2019. Anti-quenching NIR-II molecular fluorophores for in vivo high-contrast imaging and pH sensing. *Nat. Commun.* 10(1):1058
87. Zhu S, Yung BC, Chandra S, Niu G, Antaris AL, Chen X. 2018. Near-infrared-II (NIR-II) bioimaging via off-peak NIR-I fluorescence emission. *Theranostics* 8(15):4141–51
88. Staggers N, McCasky T, Brazelton N, Kennedy R. 2008. Nanotechnology: the coming revolution and its implications for consumers, clinicians, and informatics. *Nurs. Outlook* 56(5):268–74
89. Babu A, Templeton AK, Munshi A, Ramesh R. 2013. Nanoparticle-based drug delivery for therapy of lung cancer: progress and challenges. *J. Nanomater.* 2013(3):1–11
90. Sudha PN, Sangeetha K, Vijayalakshmi K, Barhoum A. 2018. Nanomaterials history, classification, unique properties, production and market. In *Emerging Applications of Nanoparticles and Architecture Nanostructures*, ed. A Barhoum, ASH Makhlouf, pp. 341–84. Amsterdam: Elsevier
91. Pokropivny VV, Skorokhod VV. 2007. Classification of nanostructures by dimensionality and concept of surface forms engineering in nanomaterial science. *Mater. Sci. Eng. C* 27(5–8):990–93
92. Teleanu DM, Chircov C, Grumezescu AM, Volceanov A, Teleanu RI. 2019. Contrast agents delivery: an up-to-date review of nanodiagnostics in neuroimaging. *Nanomaterials* 9(4):542

93. Yi G, Hong SH, Son J, Yoo J, Park C, et al. 2018. Recent advances in nanoparticle carriers for photodynamic therapy. *Quant. Imaging Med. Surg.* 8(4):433–43
94. Ananikov VP. 2019. Organic-inorganic hybrid nanomaterials. *Nanomaterials* 9(9):1197
95. Berry CC. 2012. Applications of inorganic nanoparticles for biotechnology. *Front. Nanosci.* 4:159–80
96. Casais-Molina ML, Cab C, Canto G, Medina J, Tapia A. 2018. Carbon nanomaterials for breast cancer treatment. *J. Nanomaterials* 2018:1–9
97. Albert K, Hsu H-Y. 2016. Carbon-based materials for photo-triggered theranostic applications. *Molecules* 21(11):1585
98. Pacurari M, Qian Y, Fu W, Schwegler-Berry D, Ding M, et al. 2012. Cell permeability, migration, and reactive oxygen species induced by multiwalled carbon nanotubes in human microvascular endothelial cells. *J. Toxicol. Environ. Health Part A* 75(2):112–28
99. Crouzier D, Follot S, Gentilhomme E, Flahaut E, Arnaud R, et al. 2010. Carbon nanotubes induce inflammation but decrease the production of reactive oxygen species in lung. *Toxicology* 272(1–3):39–45
100. de Melo C, Jullien M, Battie Y, En Naciri A, Ghanbaja J, et al. 2018. Tunable localized surface plasmon resonance and broadband visible photoresponse of Cu nanoparticles/ZnO surfaces. *ACS Appl. Mater. Interfaces* 10(47):40958–65
101. Attia MF, Anton N, Wallyn J, Omran Z, Vandamme TF. 2019. An overview of active and passive targeting strategies to improve the nanocarriers efficiency to tumour sites. *J. Pharm. Pharmacol.* 71(8):1185–98
102. Reimann SM, Manninen M. 2002. Electronic structure of quantum dots. *Rev. Mod. Phys.* 74(4):1283–342
103. Li Y, Yang X-Y, Feng Y, Yuan Z-Y, Su B-L. 2012. One-dimensional metal oxide nanotubes, nanowires, nanoribbons, and nanorods: synthesis, characterizations, properties and applications. *Crit. Rev. Solid State Mater. Sci.* 37(1):1–74
104. Kim H, Lee D. 2018. Near-infrared-responsive cancer photothermal and photodynamic therapy using gold nanoparticles. *Polymers* 10(9):961
105. Chen W, Ayala-Orozco C, Biswal NC, Perez-Torres C, Bartels M, et al. 2014. Targeting pancreatic cancer with magneto-fluorescent theranostic gold nanoshells. *Nanomedicine* 9(8):1209–22
106. Skrabalak SE, Chen J, Sun Y, Lu X, Au L, et al. 2008. Gold nanocages: synthesis, properties, and applications. *Acc. Chem. Res.* 41(12):1587–95
107. Ungureanu C, Kroes R, Petersen W, Groothuis TAM, Ungureanu F, et al. 2011. Light interactions with gold nanorods and cells: implications for photothermal nanotherapeutics. *Nano Lett.* 11(5):1887–94
108. Zhang Z, Wang L, Wang J, Jiang X, Li X, et al. 2012. Mesoporous silica-coated gold nanorods as a light-mediated multifunctional theranostic platform for cancer treatment. *Adv. Mater.* 24(11):1418–23
109. Phillips E, Penate-Medina O, Zanzonico PB, Carvajal RD, Mohan P, et al. 2014. Clinical translation of an ultrasmall inorganic optical-PET imaging nanoparticle probe. *Sci. Transl. Med.* 6:260ra149
110. Ge J, Jia Q, Liu W, Lan M, Zhou B, et al. 2016. Carbon dots with intrinsic theranostic properties for bioimaging, red-light-triggered photodynamic/photothermal simultaneous therapy in vitro and in vivo. *Adv. Healthc. Mater.* 5:665–75
111. Chen F, Madajewski B, Ma K, Zanoni DK, Stambuk H, et al. 2019. Molecular phenotyping and image-guided surgical treatment of melanoma using spectrally distinct ultrasmall core-shell silica nanoparticles. *Sci. Adv.* 5(12):eaax5208
112. Hong Y, Lam JWY, Tang BZ. 2011. Aggregation-induced emission. *Chem. Soc. Rev.* 40(11):5361
113. Luo J, Xie Z, Lam JWY, Cheng L, Tang BZ, et al. 2001. Aggregation-induced emission of 1-methyl-1,2,3,4,5-pentaphenylsilole. *Chem. Commun.* 2001:1740–41
114. Tang BZ, Zhao Z, Zhang H, Lam JWY. 2020. Aggregation-induced emission: new vistas at aggregate level. *Angew. Chem. Int. Ed.* 59(25):9888–907
115. Yang H, Liu Y, Guo Z, Lei B, Zhuang J, et al. 2019. Hydrophobic carbon dots with blue dispersed emission and red aggregation-induced emission. *Nat. Commun.* 10(1):1789
116. Dong J, Li X, Zhang K, Yuan YD, Wang Y, et al. 2018. Confinement of aggregation-induced emission molecular rotors in ultrathin two-dimensional porous organic nanosheets for enhanced molecular recognition. *J. Am. Chem. Soc.* 140(11):4035–46
117. Feng G, Mao D, Liu J, Goh CC, Ng LG, et al. 2018. Polymeric nanorods with aggregation-induced emission characteristics for enhanced cancer targeting and imaging. *Nanoscale* 10(13):5869–74

118. Li D, Zhao X, Qin W, Zhang H, Fei Y, et al. 2016. Toxicity assessment and long-term three-photon fluorescence imaging of bright aggregation-induced emission nanodots in zebrafish. *Nano Res.* 9(7):1921–33
119. Henson PM, Hume DA. 2006. Apoptotic cell removal in development and tissue homeostasis. *Trends Immunol.* 27(5):244–50
120. Cheng H, Wang Z, Fu L, Xu T. 2019. Macrophage polarization in the development and progression of ovarian cancers: an overview. *Front. Oncol.* 9:421
121. Negus RP, Stamp GW, Relf MG, Burke F, Malik ST, et al. 1995. The detection and localization of monocyte chemoattractant protein-1 (MCP-1) in human ovarian cancer. *J. Clin. Investig.* 95(5):2391–96
122. Kousis PC, Henderson BW, Maier PG, Gollnick SO. 2007. Photodynamic therapy enhancement of antitumor immunity is regulated by neutrophils. *Cancer Res.* 67(21):10501–10
123. Sano K, Nakajima T, Choyke PL, Kobayashi H. 2014. The effect of photoimmunotherapy (PIT) followed by liposomal daunorubicin in a mixed tumor model: a demonstration of the super enhanced permeability and retention (SUPR) effect after PIT. *Mol. Cancer Ther.* 13(2):426–32
124. Li W, Yang J, Luo L, Jiang M, Qin B, et al. 2019. Targeting photodynamic and photothermal therapy to the endoplasmic reticulum enhances immunogenic cancer cell death. *Nat. Commun.* 10(1):3349
125. Golombek SK, May J-N, Theek B, Appold L, Drude N, et al. 2018. Tumor targeting via EPR: strategies to enhance patient responses. *Adv. Drug Deliv. Rev.* 130:17–38
126. Tanaka N, Kanatani S, Tomer R, Sahlgren C, Kronqvist P, et al. 2017. Whole-tissue biopsy phenotyping of three-dimensional tumours reveals patterns of cancer heterogeneity. *Nat. Biomed. Eng.* 1(10):796–806
127. Kato A, Kataoka H, Yano S, Hayashi K, Hayashi N, et al. 2017. Maltotriose conjugation to a chlorin derivative enhances the antitumor effects of photodynamic therapy in peritoneal dissemination of pancreatic cancer. *Mol. Cancer Ther.* 16(6):1124–32
128. Tanaka M, Kataoka H, Yano S, Ohi H, Moriwaki K, et al. 2014. Antitumor effects in gastrointestinal stromal tumors using photodynamic therapy with a novel glucose-conjugated chlorin. *Mol. Cancer Ther.* 13(4):767–75
129. Yan S, Huang Q, Chen J, Song X, Chen Z, et al. 2019. Tumor-targeting photodynamic therapy based on folate-modified polydopamine nanoparticles. *Int. J. Nanomed.* 14:6799–812
130. Yoon HY, Koo H, Choi KY, Lee SJ, Kim K, et al. 2012. Tumor-targeting hyaluronic acid nanoparticles for photodynamic imaging and therapy. *Biomaterials* 33(15):3980–89
131. Aung W, Tsuji AB, Sugyo A, Takashima H, Yasunaga M, et al. 2018. Near-infrared photoimmunotherapy of pancreatic cancer using an indocyanine green-labeled anti-tissue factor antibody. *World J. Gastroenterol.* 24(48):5491–504
132. Debie P, Hernot S. 2019. Emerging fluorescent molecular tracers to guide intra-operative surgical decision-making. *Front. Pharmacol.* 10:510
133. Schmidt MM, Wittrup KD. 2009. A modeling analysis of the effects of molecular size and binding affinity on tumor targeting. *Mol. Cancer Ther.* 8(10):2861–71
134. Sano K, Nakajima T, Choyke PL, Kobayashi H. 2013. Markedly enhanced permeability and retention effects induced by photo-immunotherapy of tumors. *ACS Nano* 7(1):717–24
135. Gao W, Wang Z, Lv L, Yin D, Chen D, et al. 2016. Photodynamic therapy induced enhancement of tumor vasculature permeability using an upconversion nanoconstruct for improved intratumoral nanoparticle delivery in deep tissues. *Theranostics* 6(8):1131–44
136. Boni L, David G, Mangano A, Dionigi G, Rausei S, et al. 2015. Clinical applications of indocyanine green (ICG) enhanced fluorescence in laparoscopic surgery. *Surg. Endosc.* 29(7):2046–55
137. Henderson BW, Busch TM, Snyder JW. 2006. Fluence rate as a modulator of PDT mechanisms. *Lasers Surg. Med.* 38(5):489–93
138. Sitnik TM, Henderson BW. 1998. The effect of fluence rate on tumor and normal tissue responses to photodynamic therapy. *Photochem. Photobiol.* 67(4):462–66
139. Müller S, Walt H, Dobler-Girdziunaite D, Fiedler D, Haller U. 1998. Enhanced photodynamic effects using fractionated laser light. *J. Photochem. Photobiol. B Biol.* 42(1):67–70
140. de Bruijn HS, Brooks S, van der Ploeg-van den Heuvel A, ten Hagen TLM, de Haas ERM, Robinson DJ. 2016. Light fractionation significantly increases the efficacy of photodynamic therapy using BF-200 ALA in normal mouse skin. *PLOS ONE* 11(2):e0148850

141. Weersink RA, Bogaards A, Gertner M, Davidson SRH, Zhang K, et al. 2005. Techniques for delivery and monitoring of TOOKAD (WST09)-mediated photodynamic therapy of the prostate: clinical experience and practicalities. *J. Photochem. Photobiol. B Biol.* 79(3):211–22
142. Li J, Zhu TC. 2008. Determination of in vivo light fluence distribution in a heterogeneous prostate during photodynamic therapy. *Phys. Med. Biol.* 53(8):2103–14
143. Espina V, Mariani BD, Gallagher RI, Tran K, Banks S, et al. 2010. Malignant precursor cells pre-exist in human breast DCIS and require autophagy for survival. *PLOS ONE* 5(4):e10240
144. Smith AG, Macleod KF. 2019. Autophagy, cancer stem cells and drug resistance. *J. Pathol.* 247(5):708–18
145. Kim J, Lim W, Kim S, Jeon S, Hui Z, et al. 2014. Photodynamic therapy (PDT) resistance by PARP1 regulation on PDT-induced apoptosis with autophagy in head and neck cancer cells. *J. Oral Pathol. Med.* 43(9):675–84
146. Wei M-F, Chen M-W, Chen K-C, Lou P-J, Lin SY-F, et al. 2014. Autophagy promotes resistance to photodynamic therapy-induced apoptosis selectively in colorectal cancer stem-like cells. *Autophagy* 10(7):1179–92
147. Domagala A, Stachura J, Gabrysiak M, Muchowicz A, Zagozdzon R, et al. 2018. Inhibition of autophagy sensitizes cancer cells to Photofrin-based photodynamic therapy. *BMC Cancer* 18(1):210
148. Cincotta L, Szeto D, Lampros E, Hasan T, Cincotta AH. 1996. Benzophenothiazine and benzoporphyrin derivative combination phototherapy effectively eradicates large murine sarcomas. *Photochem. Photobiol.* 63(2):229–37
149. Chen M, Xie S. 2018. Therapeutic targeting of cellular stress responses in cancer. *Thorac. Cancer* 9(12):1575–82
150. Fahey JM, Girotti AW. 2017. Nitric oxide-mediated resistance to photodynamic therapy in a human breast tumor xenograft model: improved outcome with NOS2 inhibitors. *Nitric Oxide* 62:52–61
151. Bhowmick R, Girotti AW. 2011. Rapid upregulation of cytoprotective nitric oxide in breast tumor cells subjected to a photodynamic therapy-like oxidative challenge. *Photochem. Photobiol.* 87(2):378–86
152. Korbelik M, Parkins CS, Shibuya H, Cecic I, Stratford MRL, Chaplin DJ. 2000. Nitric oxide production by tumour tissue: impact on the response to photodynamic therapy. *Br. J. Cancer* 82(11):1835–43
153. Henderson BW, Sitnik-Busch TM, Vaughan LA. 1999. Potentiation of photodynamic therapy antitumor activity in mice by nitric oxide synthase inhibition is fluence rate dependent. *Photochem. Photobiol.* 70(1):64–71
154. Hanahan D, Weinberg RA. 2000. The hallmarks of cancer. *Cell* 100(1):57–70
155. Casas A, Di Venosa G, Hasan T, Batlle A. 2011. Mechanisms of resistance to photodynamic therapy. *Curr. Med. Chem.* 18(16):2486–515
156. Weijer R, Broekgaarden M, van Golen RF, Bulle E, Nieuwenhuis E, et al. 2015. Low-power photodynamic therapy induces survival signaling in perihilar cholangiocarcinoma cells. *BMC Cancer* 15:1014
157. Morgan J, Jackson JD, Zheng X, Pandey SK, Pandey RK. 2010. Substrate affinity of photosensitizers derived from chlorophyll-a: The ABCG2 transporter affects the phototoxic response of side population stem cell-like cancer cells to photodynamic therapy. *Mol. Pharm.* 7(5):1789–804
158. Kishen A, Upadya M, Tegos GP, Hamblin MR. 2010. Efflux pump inhibitor potentiates antimicrobial photodynamic inactivation of *Enterococcus faecalis* biofilm. *Photochem. Photobiol.* 86(6):1343–49
159. Sharkey SM, Wilson BC, Moorehead R, Singh G. 1993. Mitochondrial alterations in photodynamic therapy-resistant cells. *Cancer Res.* 53(20):4994–99
160. Shen XY, Zacal N, Singh G, Rainbow AJ. 2005. Alterations in mitochondrial and apoptosis-regulating gene expression in photodynamic therapy-resistant variants of HT29 colon carcinoma cells. *Photochem. Photobiol.* 81(2):306–13
161. Bayat Mokhtari R, Homayouni TS, Baluch N, Morgatskaya E, Kumar S, et al. 2017. Combination therapy in combating cancer. *Oncotarget* 8(23):38022–43
162. Cuperus R, van Kuilenburg ABP, Leen R, Bras J, Caron HN, Tytgat GAM. 2011. Promising effects of the 4HPR-BSO combination in neuroblastoma monolayers and spheroids. *Free Radic. Biol. Med.* 51(6):1213–20
163. Kimani SG, Phillips JB, Bruce JI, MacRobert AJ, Golding JP. 2012. Antioxidant inhibitors potentiate the cytotoxicity of photodynamic therapy. *Photochem. Photobiol.* 88(1):175–87

164. Smith D, O'Leary VJ, Darley-Usmar VM. 1993. The role of α-tocopherol as a peroxyl radical scavenger in human low density lipoprotein. *Biochem. Pharmacol.* 45:2195–201
165. Chen Q, Feng L, Liu J, Zhu W, Dong Z, et al. 2016. Intelligent albumin-MnO_2 nanoparticles as pH-/H_2O_2-responsive dissociable nanocarriers to modulate tumor hypoxia for effective combination therapy. *Adv. Mater.* 28(33):7129–36
166. Yang G, Xu L, Chao Y, Xu J, Sun X, et al. 2017. Hollow MnO_2 as a tumor-microenvironment-responsive biodegradable nano-platform for combination therapy favoring antitumor immune responses. *Nat. Commun.* 8(1):902
167. Fan H, Yan G, Zhao Z, Hu X, Zhang W, et al. 2016. A smart photosensitizer-manganese dioxide nanosystem for enhanced photodynamic therapy by reducing glutathione levels in cancer cells. *Angew. Chem. Int. Ed.* 55(18):5477–82
168. Singer E, Judkins J, Salomonis N, Matlaf L, Soteropoulos P, et al. 2015. Reactive oxygen species-mediated therapeutic response and resistance in glioblastoma. *Cell Death Dis.* 6(1):e1601
169. Ling X, Zhang S, Liu Y, Bai M. 2018. Light-activatable cannabinoid prodrug for combined and target-specific photodynamic and cannabinoid therapy. *J. Biomed. Opt.* 23(10):1–9
170. Anand S, Rollakanti KR, Horst RL, Hasan T, Maytin EV. 2014. Combination of oral vitamin D3 with photodynamic therapy enhances tumor cell death in a murine model of cutaneous squamous cell carcinoma. *Photochem. Photobiol.* 90(5):1126–35
171. Anand S, Yasinchak A, Bullock T, Govande M, Maytin EV. 2019. A non-toxic approach for treatment of breast cancer and its metastases: Capecitabine enhanced photodynamic therapy in a murine breast tumor model. *J. Cancer Metastasis Treat.* 5:6
172. Fukuhara H, Inoue K, Kurabayashi A, Furihata M, Fujita H, et al. 2013. The inhibition of ferrochelatase enhances 5-aminolevulinic acid-based photodynamic action for prostate cancer. *Photodiagn. Photodyn. Ther.* 10(4):399–409
173. Xu T, Ding W, Ji X, Ao X, Liu Y, et al. 2019. Molecular mechanisms of ferroptosis and its role in cancer therapy. *J. Cell Mol. Med.* 23(8):4900–12
174. Chen G, Guo G, Zhou X, Chen H. 2020. Potential mechanism of ferroptosis in pancreatic cancer. *Oncol. Lett.* 19(1):579–87
175. Eling N, Reuter L, Hazin J, Hamacher-Brady A, Brady NR. 2015. Identification of artesunate as a specific activator of ferroptosis in pancreatic cancer cells. *Oncoscience* 2(5):517–32
176. Anayo L, Magnussen A, Perry A, Wood M, Curnow A. 2018. An experimental investigation of a novel iron chelating protoporphyrin IX prodrug for the enhancement of photodynamic therapy. *Lasers Surg. Med.* 50(5):552–65
177. Curnow A, Perry A, Wood M. 2019. Improving in vitro photodynamic therapy through the development of a novel iron chelating aminolaevulinic acid prodrug. *Photodiagn. Photodyn Ther.* 25:157–65
178. Mrozek-Wilczkiewicz A, Malarz K, Rams-Baron M, Serda M, Bauer D, et al. 2017. Iron chelators and exogenic photosensitizers. Synergy through oxidative stress gene expression. *J. Cancer* 8(11):1979–87
179. Biswas R, Chung P-S, Moon JH, Lee S-H, Ahn J-C. 2014. Carboplatin synergistically triggers the efficacy of photodynamic therapy via caspase 3-, 8-, and 12-dependent pathways in human anaplastic thyroid cancer cells. *Lasers Med. Sci.* 29(3):995–1007
180. Cheng Y-S, Peng Y-B, Yao M, Teng J-P, Ni D, et al. 2017. Cisplatin and photodynamic therapy exert synergistic inhibitory effects on small-cell lung cancer cell viability and xenograft tumor growth. *Biochem. Biophys. Res. Commun.* 487(3):567–72
181. Ahn T-G, Jung JM, Lee E-J, Choi JH. 2019. Effects of cisplatin on photosensitizer-mediated photodynamic therapy in breast tumor-bearing nude mice. *Obstet. Gynecol. Sci.* 62(2):112–19
182. Pogue BW, O'Hara JA, Demidenko E, Wilmot CM, Goodwin IA, et al. 2003. Photodynamic therapy with verteporfin in the radiation-induced fibrosarcoma-1 tumor causes enhanced radiation sensitivity. *Cancer Res.* 63(5):1025–33
183. Xu J, Gao J, Wei Q. 2016. Combination of photodynamic therapy with radiotherapy for cancer treatment. *J. Nanomater.* 2016:8507924
184. Mroz P, Hashmi JT, Huang Y-Y, Lange N, Hamblin MR. 2011. Stimulation of anti-tumor immunity by photodynamic therapy. *Expert Rev. Clin. Immunol.* 7(1):75–91

185. Sharma P, Allison JP. 2015. The future of immune checkpoint therapy. *Science* 348(6230):56–61
186. He C, Duan X, Guo N, Chan C, Poon C, et al. 2016. Core-shell nanoscale coordination polymers combine chemotherapy and photodynamic therapy to potentiate checkpoint blockade cancer immunotherapy. *Nat. Commun.* 7:12499
187. Castano AP, Hamblin MR. 2006. Immune stimulation and photodynamic therapy to treat a metastatic model of breast cancer. *Cancer Res.* 66(8 Suppl.):1122–23
188. Li X, Le H, Wolf RF, Chen VA, Sarkar A, et al. 2011. Long-term effect on EMT6 tumors in mice induced by combination of laser immunotherapy and surgery. *Integr. Cancer Ther.* 10(4):368–73
189. Schweitzer VG. 2001. Photofrin-mediated photodynamic therapy for treatment of aggressive head and neck nonmelanomatous skin tumors in elderly patients. *Laryngoscope* 111(6):1091–98
190. Shishkova N, Kuznetsova O, Berezov T. 2012. Photodynamic therapy for gynecological diseases and breast cancer. *Cancer Biol. Med.* 9(1):9–17
191. Cramer SW, Chen CC. 2020. Photodynamic therapy for the treatment of glioblastoma. *Front. Surg.* 6:81
192. Railkar R, Agarwal PK. 2018. Photodynamic therapy in the treatment of bladder cancer: past challenges and current innovations. *Eur. Urol. Focus* 4(4):509–11
193. Ericson MB, Wennberg A-M, Larkö O. 2008. Review of photodynamic therapy in actinic keratosis and basal cell carcinoma. *Ther. Clin. Risk Manag.* 4(1):1–9
194. Geavlete B, Mulţescu R, Georgescu D, Geavlete P. 2008. Hexvix blue light fluorescence cystoscopy—a promising approach in diagnosis of superficial bladder tumors. *J. Med. Life* 1(3):355–62
195. Huggett MT, Jermyn M, Gillams A, Illing R, Mosse S, et al. 2014. Phase I/II study of verteporfin photodynamic therapy in locally advanced pancreatic cancer. *Br. J. Cancer* 110(7):1698–704
196. Akimoto J. 2016. Photodynamic therapy for malignant brain tumors. *Neurol. Med. Chir.* 56(4):151–57
197. Ishida N, Osawa S, Miyazu T, Kaneko M, Tamura S, et al. 2020. Photodynamic therapy using talaporfin sodium for local failure after chemoradiotherapy or radiotherapy for esophageal cancer: a single center experience. *J. Clin. Med.* 9(5):1509
198. Sahu A, Choi WI, Lee JH, Tae G. 2013. Graphene oxide mediated delivery of methylene blue for combined photodynamic and photothermal therapy. *Biomaterials* 34(26):6239–48
199. Xie L, Wang G, Zhou H, Zhang F, Guo Z, et al. 2016. Functional long circulating single walled carbon nanotubes for fluorescent/photoacoustic imaging-guided enhanced phototherapy. *Biomaterials* 103:219–28
200. Choudhury P, Das PK. 2019. Carbon dots-stimulated amplification of aggregation-induced emission of size-tunable organic nanoparticles. *Langmuir* 35(32):10582–95
201. Shi C, Wu JB, Chu GCY, Li Q, Wang R, et al. 2014. Heptamethine carbocyanine dye-mediated near-infrared imaging of canine and human cancers through the HIF-1α/OATPs signaling axis. *Oncotarget* 5:10114–26
202. Guo W, Qiu Z, Guo C, Ding D, Li T, et al. 2017. Multifunctional theranostic agent of $Cu_2(OH)PO_4$ quantum dots for photoacoustic image-guided photothermal/photodynamic combination cancer therapy. *ACS Appl. Mater. Interfaces* 9(11):9348–58
203. Liu X, Braun GB, Qin M, Ruoslahti E, Sugahara KN. 2017. In vivo cation exchange in quantum dots for tumor-specific imaging. *Nat. Commun.* 8(1):343
204. Topete A, Alatorre-Meda M, Iglesias P, Villar-Alvarez EM, Barbosa S, et al. 2014. Fluorescent drug-loaded, polymeric-based, branched gold nanoshells for localized multimodal therapy and imaging of tumoral cells. *ACS Nano* 8(3):2725–38
205. Li Y, Tang R, Liu X, Gong J, Zhao Z, et al. 2020. Bright aggregation-induced emission nanoparticles for two-photon imaging and localized compound therapy of cancers. *ACS Nano* 14(12):16840–53
206. Dong Q, Yang H, Wan C, Zheng D, Zhou Z, et al. 2019. Her2-functionalized gold-nanoshelled magnetic hybrid nanoparticles: a theranostic agent for dual-modal imaging and photothermal therapy of breast cancer. *Nanoscale Res. Lett.* 14(1):235

Annual Review
of Biomedical
Engineering

Volume 23, 2021

Contents

Errata

An online log of corrections to *Annual Review of Biomedical Engineering* articles may be found at http://www.annualreviews.org/errata/bioeng